

Anderson's Pediatric Cardiology

FOURTH EDITION

Editor-in-Chief

Gil Wernovsky, MD, FAAP, FACC

Senior Consultant in Pediatric Cardiac Critical Care and Pediatric Cardiology
Children's National Medical Center;
Professor of Pediatrics
George Washington University School of Medicine & Health Sciences
Washington, DC

Associate Editors

Robert H. Anderson, BSc, MD, PhD (Hon), FRCPATH, FRCS Ed (Hon)

Professor
Institute of Genetic Medicine
Newcastle University
Newcastle-upon-Tyne, United Kingdom

Krishna Kumar, MD, DM

Professor and Head
Pediatric Cardiology
Amrita Institute of Medical Sciences
Amrita Vishwa Vidyapeetham
Cochin, Kerala, India

Kathleen Mussatto, PhD, RN

Nurse Scientist
Herma Heart Institute
Children's Hospital of Wisconsin;
Associate Adjunct Professor of Cardiothoracic Surgery
Medical College of Wisconsin
Milwaukee, Wisconsin

Andrew N. Redington, MD

Chief of Cardiology
Heart Institute
Cincinnati Children's Hospital Medical Center
Cincinnati, Ohio

James S. Tweddell, MD

Chair of Cardiothoracic Surgery
Department of Surgery
Cincinnati Children's Hospital Medical Center;
Professor of Surgery and Pediatrics
University of Cincinnati
Cincinnati, Ohio

Video Editor

Justin T. Tretter, MD

Assistant Professor of Pediatrics
The Heart Institute
Cincinnati Children's Hospital Medical Center
Cincinnati, Ohio



ELSEVIER

SECTION 1

Structural and Functional Development, 1

- 1 *Terminology*, 3
ROBERT H. ANDERSON and DIANE E. SPICER
- 2 *Anatomy*, 17
ROBERT H. ANDERSON, DIANE E. SPICER, and SHUMPEI MORI
- 3 *Embryology of the Heart*, 33
ROBERT H. ANDERSON, NIGEL A. BROWN, and TIMOTHY J. MOHUN
- 4 *Etiology of Congenital Cardiac Disease*, 49
BENOIT G. BRUNEAU, DEEPAK SRIVASTAVA, and JOHN BURN
- 5 *Myocardium and Development*, 59
JEFFREY ROBBINS and JEANNE JAMES
- 6 *Physiology of the Developing Heart*, 83
HELENA M. GARDINER

SECTION 2

Prenatal Congenital Heart Disease, 109

- 7 *Magnetic Resonance Assessment of the Fetal Circulation in Congenital Heart Disease*, 111
MIKE SEED
- 8 *Imaging and Quantifying the Fetal Circulation in Congenital Cardiac Disease: Ultrasound*, 125
ANITA SZWAST and JACK RYCHIK
- 9 *Pharmacologic Intervention in the Fetus*, 137
EDGAR JAEGGI and MIKE SEED
- 10 *Percutaneous Intervention in the Fetus, Including Postnatal Management*, 149
LINDSAY R. FREUD, AUDREY C. MARSHALL, and WAYNE TWORETZKY
- 11 *The Placenta in Congenital Heart Disease*, 157
DEBORAH Y. HO and JACK RYCHIK
- 12 *Optimizing Prenatal Support of the Mother and Family*, 163
ANGELA MCBRIEN, DEBRA HILTON-KAMM, and LISA K. HORNBERGER

SECTION 3

General Topics, 171

- 13 *Prevalence of Congenital Cardiac Disease*, 173
TAREK ALSAIED and BRIAN W. MCCRINDLE

- 14 *Economic Implications of Congenital Heart Disease in Developed Countries*, 185

MATTHEW E. OSTER, GABRIEL PERLOW, SCOTT D. GROSSE, NELANGI M. PINTO, and GIL WERNOVSKY

- 15 *Prematurity and Cardiac Disease*, 189

PATRICK J. MCNAMARA, REGAN E. GIESINGER, ANNA FISK, GIL WERNOVSKY, and PETER GRUBER

- 16 *Surgical Techniques*, 215

ROOSEVELT BRYANT III, JAMES A. REAGOR, GEORGE M. HOFFMAN, and JAMES S. TWEDDELL

- 17 *Diagnostic Catheterization, Including Adults With Congenital Cardiac Disease*, 237

JOHN F. RHODES JR and AMANDA S. GREEN

- 18 *Interventional Techniques*, 253

BRYAN H. GOLDSTEIN, CHRISTOPHER J. PETIT, ALISTAIR PHILLIPS, and BETSY NEWKIRK

- 19 *Cross-Sectional Echocardiography and Doppler Imaging*, 281

CONALL T. MORGAN and LUC L. MERTENS

- 20 *Three-Dimensional Echocardiography*, 309

GIRISH S. SHIRALI and JOHN SIMPSON

- 21 *Magnetic Resonance Imaging and Computed Tomography: Diagnostic Imaging, Image Management, and Assessment of Physiology and Function*, 317

ELENA G. MILANO and ANDREW M. TAYLOR

- 22 *Electrophysiology, Pacing, and Defibrillation*, 335

MITCHELL I. COHEN, SUSAN P. ETHERIDGE, and MELISSA OLEN

- 23 *Cardiopulmonary Exercise Testing*, 379

PAUL STEPHENS JR, MICHAEL G. MCBRIDE, ALEXANDER R. OPOTOWSKY, and STEPHEN M. PARIDON

- 24 *Pediatric Cardiovascular Data, Analysis, and Critical Appraisal of the Literature*, 403

KURT R. SCHUMACHER, BRIAN W. MCCRINDLE, and SARA K. PASQUALI

- 25 *Cardiovascular Risk Factors in Youth*, 423

MICHAEL KHOURY, LAURA HAYMAN, and ELAINE URBINA

SECTION 4

Specific Lesions, 439

- 26 *Isomerism of the Atrial Appendages*, 441

ROHIT S. LOOMBA, DIANE E. SPICER, LAUREN E. RACZKA, and ROBERT H. ANDERSON

- 27** *Anomalous Systemic Venous Return*, 457
SAURABH K. GUPTA, DIANE E. SPICER, ROBERT H. ANDERSON, and RYAN A. MOORE
- 28** *Pulmonary Venous Abnormalities*, 475
RACHEL D. VANDERLAAN, ROBERT H. ANDERSON, GIRISH SHIRALI, DIANE E. SPICER, ANTHONY M. HLAVACEK, and CHRISTOPHER A. CALDARONE
- 29** *Interatrial Communications*, 503
ANDREW N. REDINGTON, ROBERT H. ANDERSON, and DIANE E. SPICER
- 30** *Division of Atrial Chambers ("Cor Triatriatum")*, 517
ROBERT H. ANDERSON, DIANE E. SPICER, and ANDREW N. REDINGTON
- 31** *Atrioventricular Septal Defects*, 521
TJARK EBELS, JUSTIN T. TRETTER, DIANE E. SPICER, and ROBERT H. ANDERSON
- 32** *Ventricular Septal Defect*, 555
JUSTIN T. TRETTER, LEE BENSON, ADRIAN CRUCEAN, DIANE E. SPICER, and ROBERT H. ANDERSON
- 33** *Diseases of the Tricuspid Valve*, 585
PATRICK W. O'LEARY, JOSEPH A. DEARANI, ROBERT H. ANDERSON, DIANE E. SPICER, and DEEPAK SRIVASTAVA
- 34** *Diseases of the Mitral Valve*, 607
JEROME SOQUET, CHRISTIAN BRIZARD, ROBERT H. ANDERSON, and DIANE E. SPICER
- 35** *Tetralogy of Fallot With Pulmonary Stenosis*, 631
CHRISTIAN APITZ, ROBERT H. ANDERSON, LYNN DEES, JAMES S. TWEDDELL, DIANE E. SPICER, and ANDREW N. REDINGTON
- 36** *Tetralogy of Fallot With Pulmonary Atresia*, 653
RITU ASIJA, MICHAEL MA, LISA WISE-FABEROWSKI, LAURA PRESNELL, ROBERT H. ANDERSON, DOFF B. MCELHINNEY, and FRANK L. HANLEY
- 37** *Transposition*, 675
WILLIAM B. KYLE, CHARLES D. FRASER III, DIANE E. SPICER, ROBERT H. ANDERSON, and DANIEL J. PENNY
- 38** *Congenitally Corrected Transposition*, 697
DAVID J. BARRON, OLIVER STUMPER, WILLIAM J. BRAWN, DIANE E. SPICER, and ROBERT H. ANDERSON
- 39** *Double-Outlet Ventricle*, 715
CHRISTOPH HALLER, GLEN S. VAN ARSDELL, SHI-JOON YOO, CECILIA S.T. GEORGE-HYSLOP, DIANE E. SPICER, and ROBERT H. ANDERSON
- 40** *Common Arterial Trunk*, 741
DANIEL J. PENNY, DIANE E. SPICER, and ROBERT H. ANDERSON
- 41** *Arterial Duct: Its Persistence and Its Patency*, 755
LEE N. BENSON, DIANE E. SPICER, and ROBERT H. ANDERSON
- 42** *Pulmonary Stenosis*, 775
JEFFREY D. DAYTON, RALF J. HOLZER, and ROBERT H. ANDERSON
- 43** *Pulmonary Atresia With Intact Ventricular Septum*, 803
MICHAEL A. QUAIL, ROBERT H. ANDERSON, DIANE E. SPICER, and PIERS E.F. DAUBENEY
- 44** *Congenital Anomalies of the Aortic Valve and Left Ventricular Outflow Tract*, 819
DIANE E. SPICER, VIKTOR HRASKA, ROBERT H. ANDERSON, SALIL GINDE, and JOSEPH R. BLOCK
- 45** *Coarctation and Interrupted Aortic Arch*, 843
KYLE W. RIGGS, ROBERT H. ANDERSON, DIANE E. SPICER, and DAVID L.S. MORALES
- 46** *Congenital Coronary Anomalies*, 865
JOYCE TAWFIK JOHNSON, MATTHEW HARRIS, ROBERT H. ANDERSON, DIANE E. SPICER, MARSHALL JACOBS, JAMES S. TWEDDELL, and JULIE BROTHERS
- 47** *Vascular Rings, Pulmonary Arterial Sling, and Related Conditions*, 877
ROOSEVELT BRYANT III and SHI-JOON YOO
- 48** *Artery of the Fifth Aortic Arch*, 901
SAURABH K. GUPTA, SIMON D. BAMFORTH, and ROBERT H. ANDERSON
- 49** *Abnormal Positions and Relationships of the Heart*, 913
SHI-JOON YOO and ROBERT H. ANDERSON
- 50** *Arteriovenous Communications*, 927
SRINATH T. GOWDA, ATHAR M. QURESHI, and HENRI JUSTINO
- 51** *Other Malformations of the Ventricular Outflow Tracts*, 945
ATHAR M. QURESHI, SRINATH T. GOWDA, HENRI JUSTINO, DIANE E. SPICER, and ROBERT H. ANDERSON
- 52** *Cardiac Tumors*, 963
JUAN-CARLOS G. MUÑIZ
- 53** *Kawasaki Disease*, 979
AUDREY DIONNE, ANNETTE BAKER, and JANE W. NEWBURGER
- 54** *Acute Rheumatic Fever*, 997
ANITA SAXENA, VERA D. AIELLO, and CLEONICE MOTA
- 55** *Chronic Rheumatic Heart Disease*, 1023
BO REMENYI
- 56** *Infective Endocarditis*, 1043
GEORGI CHRISTOV, GARTH DIXON, and MARTIN KOSTOLNY
- 57** *Pericardial Diseases in Children*, 1063
SAURABH K. GUPTA
- 58** *Aortopathies in Pediatric Cardiology and Cardiac Surgery*, 1077
CHARLES D. FRASER III, LUCA A. VRICELLA, and DUKE E. CAMERON
- 59** *Cardiologic Aspects of Systemic Disease*, 1087
ROBERT ENGLISH, THOMAS MOON, and PAULETTE ANDREA KROPP

- 60** *Systemic Hypertension*, 1115
MANISH D. SINHA and CHRISTOPHER REID

SECTION 5

Heart Failure and Transplantation, 1143

- 61** *Cardiomyopathies*, 1145
CHET RIDALL VILLA and JOHN LYNN JEFFERIES
- 62** *Cardio-oncology*, 1167
THOMAS D. RYAN
- 63** *Myocarditis*, 1173
DEEPA MOKSHAGUNDAM and JOHN TORREY BERGER III
- 64** *Acute Circulatory Failure: Pharmacologic and Mechanical Support*, 1179
SAUL FLORES, BARBARA A. ELIAS, and LARA S. SHEKERDEMIAN
- 65** *Chronic Heart Failure: Physiology and Treatment*, 1193
ROBERT E. SHADDY and DANIEL J. PENNY
- 66** *Chronic Mechanical Circulatory Support*, 1205
JOSEPH W. ROSSANO, KYLE W. RIGGS, KELLEY D. MILLER, and DAVID L.S. MORALES
- 67** *Heart and Heart-Lung Transplantation*, 1217
ANNE I. DIPCHAND, JULIE SCHMIDT, and RICHARD KIRK

SECTION 6

Functionally Univentricular Heart, 1241

- 68** *Introduction: The "Fontan Pathway,"* 1243
GIL WERNOVSKY and JAMES S. TWEDDELL
- 69** *Anatomic Considerations in the Functionally Univentricular Heart*, 1245
ROBERT H. ANDERSON and DIANE E. SPICER
- 70** *Physiologic Principles to Maximize Outcome in Patients With a Functionally Univentricular Heart*, 1261
GIL WERNOVSKY and JAMES S. TWEDDELL
- 71** *Fontan Pathway From Birth Through Early Childhood*, 1273
JAMES S. TWEDDELL, RONALD A. BRONICKI, JOSHUA W. SALVIN, MARYAM Y. NAIM, CHRISTINE M. RILEY, and GIL WERNOVSKY
- 72** *Interstage Management*, 1307
NANCY S. GHANAYEM, NANCY A. RUDD, DAVID W. BROWN, and JAMES S. TWEDDELL
- 73** *Longer-Term Outcomes and Management for Patients With a Functionally Univentricular Heart*, 1317
THOMAS L. GENTLES, CHIN LENG POH, KATHRYN RICE, YVES D'UDEKEM, LUCIANA MARCONDES, JONATHAN SKINNER, NADINE A. KASPARIAN, DAVID J. GOLDBERG, MAAN JOKHADAR, and CARL L. BACKER

SECTION 7

Beyond the Heart, 1353

- 74** *Systemic Circulation*, 1355
YIU-FAI CHEUNG
- 75** *Pulmonary Hypertension*, 1381
BRYAN SIEGEL and JOHN TORREY BERGER III
- 76** *Neurodevelopmental and Psychosocial Outcomes in Children and Young Adults With Complex Congenital Cardiac Disease*, 1393
ANNE C. SCHMELZER, GIL WERNOVSKY, DANIEL J. LICHT, and BRADLEY S. MARINO
- 77** *Congenital Cardiac Disease in the Setting of Genetic Syndromes*, 1407
M. CRISTINA DIGILIO, GIULIO CALCAGNI, MARTA UNOLT, PAOLO VERSACCI, and BRUNO MARINO
- 78** *Acute and Chronic Renal Consequences of Cardiac Disease in Children*, 1421
STUART L. GOLDSTEIN
- 79** *Pharmacogenetics in the Treatment of Congenital and Acquired Cardiac Disease During Childhood*, 1429
JONATHAN WAGNER
- 80** *Pregnancy and Congenital Heart Disease*, 1441
CANDACE SILVERSIDES, MATHEW SERMER, JACK M. COLMAN, and SAMUEL SIU
- 81** *Preparing the Young Adult With Complex Congenital Cardiac Disease to Transfer From Pediatric to Adult Care*, 1451
PHILIP MOONS
- 82** *Psychological and Social Aspects of Pediatric Cardiac Disease*, 1455
KATHLEEN MUSSATTO and ELISABETH M.W.J. UTENS
- 83** *Ethical Issues in Pediatric Cardiology and Congenital Heart Disease*, 1465
ROXANNE KIRSCH, MARA KOFFARNUS, and VANESSA MADRIGAL
- 84** *Clinical Care Pathways Supporting the Care of Children and Young People With Congenital Heart Disease*, 1481
LIZ SMITH
- 85** *Discharge Planning, Communications With the Team Providing Care in the Ambulatory Setting and the "Medical Home,"* 1487
PAUL STEPHENS JR, TYRA BRYANT-STEPHENS, JENA TANEM, and GIL WERNOVSKY
- 86** *Growth and Nutrition*, 1495
MELANIE LYN SAVOCA and SARAH PROCHASKA DAVIS

- 87** *Quality Improvement in Congenital Cardiac Disease*, 1505
JEFFREY ANDERSON, GEORGE VERGHESE, STACEY LIHN,
JAMES S. TWEDDELL, KATHERINE E. BATES, MICHAEL REBOLLEDO, and
CAROLE LANNON
- 88** *Global Burden of Pediatric Heart Disease and Pediatric Cardiac Care in Low- and Middle-Income Countries*, 1519
KRISHNA KUMAR, PARVATHI IYER, KRISHNA IYER, and
CHRISTOPHER HUGO-HAMMAN
- 89** *Screening in Pediatric and Congenital Cardiac Disease*, 1535
JOYCE T. JOHNSON, JOSEPH A. CAMARDA, GREGORY WEBSTER,
AHMAD SAMI CHAOUKI, GUILHERME BAPTISTA DE FARIA,
AMANDA M. PERAK, KIONA ALLEN, BRADLEY S. MARINO, and
STUART BERGER
- 90** *Anesthetic Considerations for Cardiac and Noncardiac Surgery in the Child With Congenital Cardiac Disease*, 1547
KELLY L. GROGAN and ANDREAS W. LOEPKE
- 91** *Telemedicine in Pediatric Cardiology*, 1553
GARY SATOU, SANKET SHAH, and CRAIG SABLE
- Index*, 1561

Video Contents

Chapter 6

- Video 6.1** Normal cord coiling, *Helena M. Gardiner*
- Video 6.2** Venous duct flow, *Helena M. Gardiner*
- Video 6.3** Flow across the oval foramen, *Helena M. Gardiner*
- Video 6.4** Pulmonary veins, *Helena M. Gardiner*
- Video 6.5** Aortic isthmus, *Helena M. Gardiner*
- Video 6.6** Arterial duct, *Helena M. Gardiner*
- Video 6.7** Reversal of flow in aortic isthmus in a growth-restricted fetus, *Helena M. Gardiner*
- Video 6.8** High-resolution microscopic episcopy at 11 weeks' gestation, *Helena M. Gardiner*
- Video 6.9** Severe tricuspid regurgitation in a fetus with pulmonary atresia, *Helena M. Gardiner*
- Video 6.10** Vein of Galen malformation, *Helena M. Gardiner*
- Video 6.11** Coronary flow in a fetus with twin-to-twin transfusion, *Helena M. Gardiner*
- Video 6.12** Bidirectional coronary flow in a fetus with pulmonary atresia with intact ventricular septum and ventriculocoronary fistula, *Helena M. Gardiner*
- Video 6.13** Aortic coarctation, *Helena M. Gardiner*

Chapter 7

- Video 7.1** Streaming in the fetal circulation by MRI 4D flow, *Mike Seed*
- Video 7.2** MRI of a fetus with transposition of the great arteries, *Mike Seed*

Chapter 8

- Video 8.1** Color Doppler interrogation of the ductal arch demonstrating aliasing of the duct at the insertion into the descending aorta, *Anita Szwast, Jack Rychik*
- Video 8.2** 2D imaging of the four-chamber view of the heart demonstrating right ventricular dilation and hypertrophy with poor systolic function, *Anita Szwast, Jack Rychik*
- Video 8.3** Color Doppler interrogation of the tricuspid valve demonstrating moderate tricuspid valve regurgitation, *Anita Szwast, Jack Rychik*
- Video 8.4** Color Doppler interrogation of the pulmonary valve demonstrating mild pulmonary insufficiency, *Anita Szwast, Jack Rychik*
- Video 8.5** 2D imaging of a fetus with hypoplastic left heart syndrome, *Anita Szwast, Jack Rychik*
- Video 8.6** Left-to-right flow across the patent oval foramen and trivial tricuspid regurgitation, *Anita Szwast, Jack Rychik*
- Video 8.7** Color Doppler interrogation of the aortic arch demonstrating aortic arch hypoplasia with all retrograde flow, *Anita Szwast, Jack Rychik*
- Video 8.8** 2D and color Doppler interrogation of a fetus with critical aortic stenosis, *Anita Szwast, Jack Rychik*
- Video 8.9** Color Doppler interrogation of the aortic valve, *Anita Szwast, Jack Rychik*
- Video 8.10** 2D imaging of the four-chamber view of the heart, *Anita Szwast, Jack Rychik*

- Video 8.11** 2D imaging of the aortic arch demonstrating moderate to severe transverse aortic arch and isthmal hypoplasia, *Anita Szwast, Jack Rychik*
- Video 8.12** Color Doppler interrogation of the aortic arch demonstrating reversal of flow in the distal transverse aortic arch, *Anita Szwast, Jack Rychik*
- Video 8.13** 2D imaging demonstrating the atretic tricuspid valve with hypoplastic right ventricle, *Anita Szwast, Jack Rychik*
- Video 8.14** 2D color Doppler interrogation of the main pulmonary artery and arterial duct, *Anita Szwast, Jack Rychik*
- Video 8.15** Color Doppler interrogation of the branch pulmonary arteries, which are mildly hypoplastic, *Anita Szwast, Jack Rychik*
- Video 8.16** Color Doppler interrogation of the aortic arch demonstrating the arterial duct arising from the underside of the aortic arch, *Anita Szwast, Jack Rychik*
- Video 8.17** 2D imaging of the aortic outflow tract demonstrating the ventricular septal defect and overriding aorta, *Anita Szwast, Jack Rychik*
- Video 8.18** Color Doppler interrogation of the aortic outflow tract demonstrating flow from both ventricles across the aortic valve, *Anita Szwast, Jack Rychik*
- Video 8.19** 2D imaging of the right ventricular outflow tract demonstrating the anterior deviation of the outlet septum, *Anita Szwast, Jack Rychik*
- Video 8.20** 2D imaging of the tricuspid valve demonstrating a dysplastic tricuspid valve, *Anita Szwast, Jack Rychik*
- Video 8.21** Color Doppler interrogation of the tricuspid valve demonstrating severe tricuspid regurgitation, *Anita Szwast, Jack Rychik*
- Video 8.22** Color Doppler interrogation of the pulmonary valve, *Anita Szwast, Jack Rychik*
- Video 8.23** Color Doppler interrogation of the aortic arch and arterial duct demonstrating a tortuous arterial duct with all retrograde flow, *Anita Szwast, Jack Rychik*
- Video 8.24** 2D imaging of the four-chamber view, *Anita Szwast, Jack Rychik*
- Video 8.25** 2D imaging of the outflow tracts and ductal and aortic arches, *Anita Szwast, Jack Rychik*
- Video 8.26** 2D imaging of the outflow tracts demonstrating that the pulmonary artery arises from the left ventricle while the aorta arises from the right ventricle, *Anita Szwast, Jack Rychik*

Chapter 9

- Video 9.1** Short VA tachycardia, *Edgar Jaeggi, Mike Seed*
- Video 9.2** Long VA tachycardia, *Edgar Jaeggi, Mike Seed*
- Video 9.3** Atrial flutter, *Edgar Jaeggi, Mike Seed*
- Video 9.4** Antibody-mediated complete heart block, *Edgar Jaeggi, Mike Seed*

Chapter 10

- Video 10.1** Needle insertion for fetal aortic valvuloplasty, *Lindsay R. Freud, Audrey C. Marshall, Wayne Tworetzky*
- Video 10.2** Balloon dilation for fetal aortic valvuloplasty, *Lindsay R. Freud, Audrey C. Marshall, Wayne Tworetzky*

Video 10.3 **Technical success with aortic regurgitation,** *Lindsay R. Freud, Audrey C. Marshall, Wayne Tworetzky*

Video 10.4 **Balloon dilation for fetal pulmonary valvuloplasty,** *Lindsay R. Freud, Audrey C. Marshall, Wayne Tworetzky*

Video 10.5 **Atrial septal stent placement,** *Lindsay R. Freud, Audrey C. Marshall, Wayne Tworetzky*

Chapter 16

Video 16.1 **Basics of cardiopulmonary bypass,** *James Reagor*

Chapter 19

Video 19.1 **Abdominal situs sweep,** *Luc Mertens, Robert H. Anderson, Diane E. Spicer, Conall Morgan*

Video 19.2 **Abdominal situs sweep with color,** *Luc Mertens, Robert H. Anderson, Diane E. Spicer, Conall Morgan*

Video 19.3 **Inferior caval vein in long axis seen traversing the liver and entering the right atrium,** *Luc Mertens, Robert H. Anderson, Diane E. Spicer, Conall Morgan*

Video 19.4 **Inferior caval vein in long axis with color,** *Luc Mertens, Robert H. Anderson, Diane E. Spicer, Conall Morgan*

Video 19.5 **Abdominal aorta in long axis,** *Luc Mertens, Robert H. Anderson, Diane E. Spicer, Conall Morgan*

Video 19.6 **Abdominal aorta in long axis with color,** *Luc Mertens, Robert H. Anderson, Diane E. Spicer, Conall Morgan*

Video 19.7 **Subcostal long-axis sweep from posterior to anterior,** *Luc Mertens, Robert H. Anderson, Diane E. Spicer, Conall Morgan*

Video 19.8 **Subcostal long-axis sweep with color,** *Luc Mertens, Robert H. Anderson, Diane E. Spicer, Conall Morgan*

Video 19.9 **Subcostal short-axis sweep,** *Luc Mertens, Robert H. Anderson, Diane E. Spicer, Conall Morgan*

Video 19.10 **Subcostal short-axis sweep with color,** *Luc Mertens, Robert H. Anderson, Diane E. Spicer, Conall Morgan*

Video 19.11 **Subcostal view of the atrial septum,** *Luc Mertens, Robert H. Anderson, Diane E. Spicer, Conall Morgan*

Video 19.12 **Subcostal view of the intraatrial septum with color,** *Luc Mertens, Robert H. Anderson, Diane E. Spicer, Conall Morgan*

Video 19.13 **Bicaval view of the superior and inferior caval veins as well as the atrial septum,** *Luc Mertens, Robert H. Anderson, Diane E. Spicer, Conall Morgan*

Video 19.14 **Subcostal right ventricular outflow tract view,** *Luc Mertens, Robert H. Anderson, Diane E. Spicer, Conall Morgan*

Video 19.15 **Subcostal right ventricular outflow tract view with color,** *Luc Mertens, Robert H. Anderson, Diane E. Spicer, Conall Morgan*

Video 19.16 **Subcostal left ventricular outflow tract view,** *Luc Mertens, Robert H. Anderson, Diane E. Spicer, Conall Morgan*

Video 19.17 **Subcostal left ventricular outflow tract view with color,** *Luc Mertens, Robert H. Anderson, Diane E. Spicer, Conall Morgan*

Video 19.18 **Parasternal long-axis view,** *Luc Mertens, Robert H. Anderson, Diane E. Spicer, Conall Morgan*

Video 19.19 **Parasternal long-axis view of the aortic valve with color,** *Luc Mertens, Robert H. Anderson, Diane E. Spicer, Conall Morgan*

Video 19.20 **Parasternal long-axis of the mitral valve with color,** *Luc Mertens, Robert H. Anderson, Diane E. Spicer, Conall Morgan*

Video 19.21 **Ascending aorta can be viewed by moving up a rib space from the parasternal long-axis view,** *Luc Mertens, Robert H. Anderson, Diane E. Spicer, Conall Morgan*

Video 19.22 **Right ventricular inflow view demonstrating the anterior and inferior leaflets of the tricuspid valve,** *Luc Mertens, Robert H. Anderson, Diane E. Spicer, Conall Morgan*

Video 19.23 **Right ventricular outflow view,** *Luc Mertens, Robert H. Anderson, Diane E. Spicer, Conall Morgan*

Video 19.24 **Right ventricular outflow view with color,** *Luc Mertens, Robert H. Anderson, Diane E. Spicer, Conall Morgan*

Video 19.25 **Right ventricular outflow view with color,** *Luc Mertens, Robert H. Anderson, Diane E. Spicer, Conall Morgan*

Video 19.26 **Parasternal long-axis sweep assessing for ventricular septal defect,** *Luc Mertens, Robert H. Anderson, Diane E. Spicer, Conall Morgan*

Video 19.27 **Parasternal short-axis view of the aortic valve en face with color,** *Luc Mertens, Robert H. Anderson, Diane E. Spicer, Conall Morgan*

Video 19.28 **Color compare of the right coronary artery ostium,** *Luc Mertens, Robert H. Anderson, Diane E. Spicer, Conall Morgan*

Video 19.29 **Color compare of the left coronary artery ostium and the left main coronary artery dividing into the left anterior descending and circumflex,** *Luc Mertens, Robert H. Anderson, Diane E. Spicer, Conall Morgan*

Video 19.30 **Mitral valve en face demonstrating both anterior and posterior leaflets,** *Luc Mertens, Robert H. Anderson, Diane E. Spicer, Conall Morgan*

Video 19.31 **Mitral valve en face with color,** *Luc Mertens, Robert H. Anderson, Diane E. Spicer, Conall Morgan*

Video 19.32 **Parasternal short-axis basal level,** *Luc Mertens, Robert H. Anderson, Diane E. Spicer, Conall Morgan*

Video 19.33 **Parasternal short-axis mid-ventricular level,** *Luc Mertens, Robert H. Anderson, Diane E. Spicer, Conall Morgan*

Video 19.34 **Parasternal short axis at the apex,** *Luc Mertens, Robert H. Anderson, Diane E. Spicer, Conall Morgan*

Video 19.35 **Parasternal short-axis sweep from the base of the heart to the apex assessing for ventricular septal defects with color,** *Luc Mertens, Robert H. Anderson, Diane E. Spicer, Conall Morgan*

Video 19.36 **High parasternal view of the branch pulmonary arteries,** *Luc Mertens, Robert H. Anderson, Diane E. Spicer, Conall Morgan*

Video 19.37 **High parasternal view of the branch pulmonary arteries with color,** *Luc Mertens, Robert H. Anderson, Diane E. Spicer, Conall Morgan*

Video 19.38 **High parasternal view of the pulmonary veins ("crab view"),** *Luc Mertens, Robert H. Anderson, Diane E. Spicer, Conall Morgan*

Video 19.39 **High parasternal view of the pulmonary veins with color,** *Luc Mertens, Robert H. Anderson, Diane E. Spicer, Conall Morgan*

Video 19.40 **Sweep through the descending aorta and left pulmonary artery assessing for a patent arterial duct,** *Luc Mertens, Robert H. Anderson, Diane E. Spicer, Conall Morgan*

Video 19.41 **Apical four-chamber view,** *Luc Mertens, Robert H. Anderson, Diane E. Spicer, Conall Morgan*

- Video 19.42** **Apical four-chamber view with color on the mitral valve**, Luc Mertens, Robert H. Anderson, Diane E. Spicer, Conall Morgan
- Video 19.43** **Apical four-chamber view with color on the tricuspid valve**, Luc Mertens, Robert H. Anderson, Diane E. Spicer, Conall Morgan
- Video 19.44** **Apical right ventricle centered view**, Luc Mertens, Robert H. Anderson, Diane E. Spicer, Conall Morgan
- Video 19.45** **Apical five-chamber view demonstrating left ventricular inflow and outflow**, Luc Mertens, Robert H. Anderson, Diane E. Spicer, Conall Morgan
- Video 19.46** **Apical five-chamber view with color**, Luc Mertens, Robert H. Anderson, Diane E. Spicer, Conall Morgan
- Video 19.47** **Apical two-chamber view**, Luc Mertens, Robert H. Anderson, Diane E. Spicer, Conall Morgan
- Video 19.48** **Apical two-chamber view with color**, Luc Mertens, Robert H. Anderson, Diane E. Spicer, Conall Morgan
- Video 19.49** **Apical three-chamber view**, Luc Mertens, Robert H. Anderson, Diane E. Spicer, Conall Morgan
- Video 19.50** **Apical three-chamber view with color**, Luc Mertens, Robert H. Anderson, Diane E. Spicer, Conall Morgan
- Video 19.51** **Sweep from the right-sided superior caval vein through the brachiocephalic vein looking for a left-sided superior caval vein**, Luc Mertens, Robert H. Anderson, Diane E. Spicer, Conall Morgan
- Video 19.52** **Determination of arch sidedness showing the ascending aorta in short axis, whose first branch passes to the patient's right, implying a left-sided aortic arch**, Luc Mertens, Robert H. Anderson, Diane E. Spicer, Conall Morgan
- Video 19.53** **Arch determination with color**, Luc Mertens, Robert H. Anderson, Diane E. Spicer, Conall Morgan
- Video 19.54** **Aortic arch in long axis showing normal branching pattern: brachiocephalic artery, left common carotid artery, and left subclavian artery**, Luc Mertens, Robert H. Anderson, Diane E. Spicer, Conall Morgan
- Video 19.55** **Aortic arch in long axis with color**, Luc Mertens, Robert H. Anderson, Diane E. Spicer, Conall Morgan

Chapter 20

- Video 20.1** **Standard grayscale view of a 3D echocardiogram**, Girish S. Shirali, John Simpson
- Video 20.2** **Enhanced depth perception using color rendering**, Girish S. Shirali, John Simpson
- Video 20.3** **Multiplanar reformatted view of atrioventricular septal defect**, Luc Mertens, Robert H. Anderson, Diane E. Spicer, Conall Morgan
- Video 20.4** **Cross-plane (simultaneous orthogonal 2D) echocardiography**, Luc Mertens, Robert H. Anderson, Diane E. Spicer, Conall Morgan
- Video 20.5** **Perimembranous ventricular septal defect viewed from the right ventricle by 3D echocardiography**, Luc Mertens, Robert H. Anderson, Diane E. Spicer, Conall Morgan
- Video 20.6** **Overgained 3D echocardiogram**, Luc Mertens, Robert H. Anderson, Diane E. Spicer, Conall Morgan
- Video 20.7** **Undergained 3D echocardiogram**, Luc Mertens, Robert H. Anderson, Diane E. Spicer, Conall Morgan
- Video 20.8** **Secundum atrial septal defect viewed from the right atrium by 3D echocardiography**, Girish S. Shirali, John Simpson

Chapter 21

- Video 21.1** **Ventricular volume measurement in a patient with hypoplastic left heart syndrome from MRI bSSFP cine images**, Elena G. Milano, Andrew M. Taylor
- Video 21.2** **MRI axial reformat of 3D bSSFP**, Elena G. Milano, Andrew M. Taylor
- Video 21.3** **MRI 3D volume-rendered bSSFP whole heart image (anterior view)**, Elena G. Milano, Andrew M. Taylor
- Video 21.4** **MRI phase contrast velocity flow measurement in the pulmonary trunk**, Elena G. Milano, Andrew M. Taylor
- Video 21.5** **MRI 4D phase contrast flow in a normal human**, Elena G. Milano, Andrew M. Taylor
- Video 21.6** **Reversible inducible ischemia seen on MRI first-pass perfusion**, Elena G. Milano, Andrew M. Taylor
- Video 21.7** **Real-time MRI radial k-t SENSE and spiral phase images**, Elena G. Milano, Andrew M. Taylor
- Video 21.8** **3D printing of the right ventricular outflow tract**, Elena G. Milano, Andrew M. Taylor
- Video 21.9** **CT scanner with casing removed showing the speed at which modern spiral CT scanners rotate**, Elena G. Milano, Andrew M. Taylor
- Video 21.10** **MRI machine**, Elena G. Milano, Andrew M. Taylor
- Video 21.11** **3D volume-rendered contrast-enhanced cardiac CT showing an anomalous left coronary artery from the pulmonary artery**, Elena G. Milano, Andrew M. Taylor
- Video 21.12** **4D volume-rendered contrast enhanced cardiac CT of the right ventricular outflow tract**, Elena G. Milano, Andrew M. Taylor

Chapter 22

- Video 22.1** **Sinus rhythm activation**, Mitchell Cohen, Susan Etheridge, Melissa Olen
- Video 22.2** **Propagation map of typical atrial flutter**, Mitchell Cohen, Susan Etheridge, Melissa Olen
- Video 22.3** **Propagation map of double loop atrial flutter**, Mitchell Cohen, Susan Etheridge, Melissa Olen

Chapter 27

- Video 27.1** **Angiogram in a patient with bilateral superior caval veins showing the presence of a connecting brachiocephalic vein**, Saurabh K. Gupta, Diane E. Spicer, Robert H. Anderson, Ryan Moore
- Video 27.2** **Echocardiographic subcostal parasagittal view of azygous continuation of the inferior caval vein**, Saurabh K. Gupta, Diane E. Spicer, Robert H. Anderson, Ryan Moore
- Video 27.3** **Angiogram of right superior caval vein connected to morphologic left atrium**, Saurabh K. Gupta, Diane E. Spicer, Robert H. Anderson, Ryan Moore
- Video 27.4** **Saline contrast echocardiogram in apical plane in a child with persistent left superior caval vein draining directly to the left atrium**, Saurabh K. Gupta, Diane E. Spicer, Robert H. Anderson, Ryan Moore
- Video 27.5** **Saline contrast echocardiography performed after an injection of agitated saline in the left antecubital vein**, Saurabh K. Gupta, Diane E. Spicer, Robert H. Anderson, Ryan Moore
- Video 27.6** **Saline contrast echocardiography performed after an injection of agitated saline in the left antecubital vein**, Saurabh K. Gupta, Diane E. Spicer, Robert H. Anderson, Ryan Moore

Chapter 28

- Video 28.1** 3D CT reconstruction of mixed total anomalous pulmonary venous connection, *Rachel Vanderlaan*
- Video 28.2** 3D CT reconstruction of supracardiac total anomalous pulmonary venous connection, *Rachel Vanderlaan*
- Video 28.3** 3D CT reconstruction of infracardiac total anomalous pulmonary venous connection, *Rachel Vanderlaan*
- Video 28.4** Echocardiography of cardiac total anomalous pulmonary venous drainage, *Rachel Vanderlaan*
- Video 28.5** Echocardiography of cardiac total anomalous pulmonary venous drainage, *Rachel Vanderlaan*
- Video 28.6** Echocardiography color Doppler of supracardiac total anomalous pulmonary venous drainage, *Rachel Vanderlaan*
- Video 28.7** 3D CT reconstruction of mixed total anomalous pulmonary venous drainage, *Rachel Vanderlaan*
- Video 28.8** Infradiaphragmatic total anomalous pulmonary venous connection repair and patch closure of atrial septal defect, *Rachel Vanderlaan*
- Video 28.9** 3D CT reconstruction of isolated pulmonary venous stenosis, *Rachel Vanderlaan*

Chapter 29

- Video 29.1** Small-moderate secundum atrial septal defect, echocardiography, subcostal short axis, *Andrew Redington, Robert H. Anderson*
- Video 29.2** Small-moderate secundum atrial septal defect, shunting left to right, *Andrew Redington, Robert H. Anderson*
- Video 29.3** Small-moderate secundum atrial septal defect, echocardiography, subcostal long axis, *Andrew Redington, Robert H. Anderson*
- Video 29.4** Superior sinus venosus defect with anomalous right upper pulmonary vein above superior caval vein—right atrial junction, echocardiography subcostal short-axis plane with color Doppler, *Andrew Redington, Robert H. Anderson*
- Video 29.5** Vestibular defect with additional oval fossa defect: transesophageal echocardiographic color comparison, *Andrew Redington, Robert H. Anderson*
- Video 29.6** Vestibular atrial septal defect with bidirectional shunting: transesophageal color comparison, *Andrew Redington, Robert H. Anderson*
- Video 29.7** Fenestrated secundum atrial septal defect, echocardiography subcostal long axis with color Doppler, *Andrew Redington, Robert H. Anderson*
- Video 29.8** Fenestrated secundum atrial septal defect, echocardiography subcostal short axis with color Doppler, *Andrew Redington, Robert H. Anderson*
- Video 29.9** Secundum atrial septal defect patch closure (bovine pericardium), *Andrew Redington, Robert H. Anderson*
- Video 29.10** Sinus venosus defect with partial anomalous venous connection, two-patch repair, *Andrew Redington, Robert H. Anderson*
- Video 29.11** Status post 30 mm Gore Cardioform Septal Occluder: transesophageal echocardiogram, *Andrew Redington, Robert H. Anderson*

Chapter 30

- Video 30.1** Division of the right atrium, echocardiography apical view, *Robert H. Anderson, Diane E. Spicer, Andrew N. Redington*

Chapter 31

- Video 31.1** Unwedged position of the aortic root, echocardiography, *Tjark Ebels, Justin T. Tretter, Diane E. Spicer, Robert H. Anderson*
- Video 31.2** Counterclockwise rotated orientation of the left ventricular papillary muscles, echocardiography, *Tjark Ebels, Justin T. Tretter, Diane E. Spicer, Robert H. Anderson*
- Video 31.3** Common atrioventricular valve regurgitation, echocardiography, *Tjark Ebels, Justin T. Tretter, Diane E. Spicer, Robert H. Anderson*
- Video 31.4** Atrioventricular septal defect with exclusively atrial level shunting, echocardiography, *Tjark Ebels, Justin T. Tretter, Diane E. Spicer, Robert H. Anderson*
- Video 31.5** Atrioventricular septal defect with large atrial and small restrictive ventricular level shunting, echocardiography, *Tjark Ebels, Justin T. Tretter, Diane E. Spicer, Robert H. Anderson*
- Video 31.6** Atrioventricular septal defect with large atrial and ventricular level shunting, echocardiography, *Tjark Ebels, Justin T. Tretter, Diane E. Spicer, Robert H. Anderson*
- Video 31.7** Subcostal long-axis echocardiographic plane to view atrial component of atrioventricular septal defect, *Tjark Ebels, Justin T. Tretter, Diane E. Spicer, Robert H. Anderson*
- Video 31.8** Atrioventricular septal defect with separate atrioventricular valvar orifices, echocardiography, *Tjark Ebels, Justin T. Tretter, Diane E. Spicer, Robert H. Anderson*
- Video 31.9** Dual orifice left atrioventricular valve, 3D echocardiography, *Tjark Ebels, Justin T. Tretter, Diane E. Spicer, Robert H. Anderson*
- Video 31.10** Dual orifice left atrioventricular valve, echocardiography, *Tjark Ebels, Justin T. Tretter, Diane E. Spicer, Robert H. Anderson*
- Video 31.11** Modified subcostal echocardiographic view for profiling the common atrioventricular valve, Rastelli type A, *Tjark Ebels, Justin T. Tretter, Diane E. Spicer, Robert H. Anderson*
- Video 31.12** Modified subcostal echocardiographic view for profiling the common atrioventricular valve, Rastelli type B, *Tjark Ebels, Justin T. Tretter, Diane E. Spicer, Robert H. Anderson*
- Video 31.13** Modified subcostal echocardiographic view for profiling the common atrioventricular valve, Rastelli type C, *Tjark Ebels, Justin T. Tretter, Diane E. Spicer, Robert H. Anderson*
- Video 31.14** Severe left atrioventricular valve regurgitation status post repair, echocardiography, *Tjark Ebels, Justin T. Tretter, Diane E. Spicer, Robert H. Anderson*
- Video 31.15** Left atrioventricular valve stenosis status post repair, echocardiography, *Tjark Ebels, Justin T. Tretter, Diane E. Spicer, Robert H. Anderson*
- Video 31.16** 3D echocardiography demonstrating separate atrioventricular valve orifices, *Tjark Ebels, Justin T. Tretter, Diane E. Spicer, Robert H. Anderson*
- Video 31.17** 3D echocardiography demonstrating a common atrioventricular valve, Rastelli type A, *Tjark Ebels, Justin T. Tretter, Diane E. Spicer, Robert H. Anderson*
- Video 31.18** 3D echocardiography demonstrating a common atrioventricular valve, Rastelli type C, *Tjark Ebels, Justin T. Tretter, Diane E. Spicer, Robert H. Anderson*

Video 31.19 Two-patch repair of atrioventricular septal defect, Tjark Ebels, Justin T. Tretter, Diane E. Spicer, Robert H. Anderson

Video 31.20 Two-patch repair of atrioventricular septal defect, Tjark Ebels, Justin T. Tretter, Diane E. Spicer, Robert H. Anderson

Chapter 32

Video 32.1 Perimembranous central defect, echocardiography in parasternal short axis, Justin T. Tretter, Lee Benson, Adrian Crucean, Diane E. Spicer, Robert H. Anderson

Video 32.2 Perimembranous central defect, echocardiography in subcostal short axis, Justin T. Tretter, Lee Benson, Adrian Crucean, Diane E. Spicer, Robert H. Anderson

Video 32.3 Perimembranous inlet defect, echocardiography in apical plane, Justin T. Tretter, Lee Benson, Adrian Crucean, Diane E. Spicer, Robert H. Anderson

Video 32.4 Perimembranous inlet defect, color Doppler echocardiography in subcostal short axis, Justin T. Tretter, Lee Benson, Adrian Crucean, Diane E. Spicer, Robert H. Anderson

Video 32.5 Perimembranous inlet defect with malalignment between the atrial and muscular ventricular septa, echocardiography in apical plane, Justin T. Tretter, Lee Benson, Adrian Crucean, Diane E. Spicer, Robert H. Anderson

Video 32.6 Perimembranous inlet defect, echocardiography in apical plane sweeping to the aortic valve, Justin T. Tretter, Lee Benson, Adrian Crucean, Diane E. Spicer, Robert H. Anderson

Video 32.7 Muscular inlet defect, echocardiography in apical plane, Justin T. Tretter, Lee Benson, Adrian Crucean, Diane E. Spicer, Robert H. Anderson (Courtesy James S. Tweddell)

Video 32.8 Muscular inlet defect, echocardiography in subcostal short-axis plane, Justin T. Tretter, Lee Benson, Adrian Crucean, Diane E. Spicer, Robert H. Anderson

Video 32.9 Perimembranous outlet defect with anterior deviation of the outlet septum, echocardiography in parasternal short axis, Justin T. Tretter, Lee Benson, Adrian Crucean, Diane E. Spicer, Robert H. Anderson

Video 32.10 Perimembranous outlet defect with posterior deviation of the outlet septum, echocardiography in parasternal long axis, Justin T. Tretter, Lee Benson, Adrian Crucean, Diane E. Spicer, Robert H. Anderson

Video 32.11 Perimembranous outlet defect with posterior deviation of the outlet septum, echocardiography in parasternal short axis, Justin T. Tretter, Lee Benson, Adrian Crucean, Diane E. Spicer, Robert H. Anderson

Video 32.12 Apical muscular defects, color Doppler comparison echocardiography in apical plane, Justin T. Tretter, Lee Benson, Adrian Crucean, Diane E. Spicer, Robert H. Anderson

Video 32.13 Doubly committed defect, color Doppler comparison echocardiography in parasternal short axis, Justin T. Tretter, Lee Benson, Adrian Crucean, Diane E. Spicer, Robert H. Anderson

Video 32.14 Doubly committed defect with perimembranous extension, echocardiography in parasternal short axis, Justin T. Tretter, Lee Benson, Adrian Crucean, Diane E. Spicer, Robert H. Anderson

Video 32.15 Prolapse of the right coronary leaflet through a perimembranous defect, echocardiography in parasternal long axis, Justin T. Tretter, Lee Benson, Adrian Crucean, Diane E. Spicer, Robert H. Anderson

Video 32.16 Spontaneous closure of a perimembranous defect evident in parasternal long-axis echocardiography, Justin T. Tretter, Lee Benson, Adrian Crucean, Diane E. Spicer, Robert H. Anderson

Video 32.17 Perimembranous ventricular septal defect patch closure surgery, Justin T. Tretter, Lee Benson, Adrian Crucean, Diane E. Spicer, Robert H. Anderson

Chapter 33

Video 33.1 Tricuspid valve in Ebstein malformation, echocardiography in apical plane, Patrick W. O'Leary, Joseph A. Dearani, Robert H. Anderson, Diane E. Spicer

Video 33.2 Tricuspid valve in Ebstein malformation, echocardiography apical plane with color Doppler, Patrick W. O'Leary, Joseph A. Dearani, Robert H. Anderson, Diane E. Spicer

Video 33.3 Tricuspid valve in Ebstein malformation after cone reconstruction, echocardiography in apical plane, Patrick W. O'Leary, Joseph A. Dearani, Robert H. Anderson, Diane E. Spicer

Video 33.4 Tricuspid valve in Ebstein malformation after cone reconstruction, echocardiography in apical plane with color Doppler, Patrick W. O'Leary, Joseph A. Dearani, Robert H. Anderson, Diane E. Spicer

Video 33.5 Tricuspid valve in Ebstein malformation after cone reconstruction, echocardiography in short-axis plane, Patrick W. O'Leary, Joseph A. Dearani, Robert H. Anderson, Diane E. Spicer

Video 33.6 Tricuspid valve in Ebstein malformation after cone reconstruction, echocardiography in short-axis plane with color Doppler, Patrick W. O'Leary, Joseph A. Dearani, Robert H. Anderson, Diane E. Spicer

Video 33.7 Cone reconstruction in Ebstein malformation, Patrick W. O'Leary, Joseph A. Dearani, Robert H. Anderson, Diane E. Spicer

Chapter 35

Video 35.1 Parasternal long-axis echocardiogram demonstrating the aortic valve overriding the crest of the muscular ventricular septum, Christian Apitz, Robert H. Anderson, Lynn Dees, James S. Tweddell, Diane E. Spicer, Andrew N. Redington

Video 35.2 Modified parasternal long-axis echocardiogram demonstrating the anatomy of right ventricular outflow tract obstruction, the right ventricle-pulmonary artery junction (annulus), and valvar morphology, Christian Apitz, Robert H. Anderson, Lynn Dees, James S. Tweddell, Diane E. Spicer, Andrew N. Redington

Video 35.3 Parasternal short-axis echocardiogram showing the size and position of the ventricular septal defect, shunting direction, and the anatomy of right ventricular outflow tract obstruction, Christian Apitz, Robert H. Anderson, Lynn Dees, James S. Tweddell, Diane E. Spicer, Andrew N. Redington

Video 35.4 Five-chamber echocardiogram demonstrating size and position of the ventricular septal defect, shunting direction, and degree of overriding of aorta, Christian Apitz, Robert H. Anderson, Lynn Dees, James S. Tweddell, Diane E. Spicer, Andrew N. Redington

Video 35.5 Five-chamber echocardiogram of a newborn with tetralogy of Fallot presenting with cyanosis and arterial hypotension, Christian Apitz, Robert H. Anderson, Lynn Dees, James S. Tweddell, Diane E. Spicer, Andrew N. Redington

- Video 35.6 Parasternal long-axis echocardiogram of a newborn with tetralogy of Fallot presenting with cyanosis and arterial hypotension**, *Christian Apitz, Robert H. Anderson, Lynn Dees, James S. Tweddell, Diane E. Spicer, Andrew N. Redington*
- Video 35.7 Parasternal short-axis echocardiogram of a newborn with tetralogy of Fallot presenting with cyanosis and arterial hypotension**, *Christian Apitz, Robert H. Anderson, Lynn Dees, James S. Tweddell, Diane E. Spicer, Andrew N. Redington*
- Video 35.8 High parasternal short-axis echocardiogram**, *Christian Apitz, Robert H. Anderson, Lynn Dees, James S. Tweddell, Diane E. Spicer, Andrew N. Redington*
- Video 35.9 High parasternal short-axis echocardiogram showing the rudimentary nature of the leaflets of the pulmonary valve**, *Christian Apitz, Robert H. Anderson, Lynn Dees, James S. Tweddell, Diane E. Spicer, Andrew N. Redington*
- Video 35.10 MRI four-chamber view of a patient with tetralogy of Fallot**, *Christian Apitz, Robert H. Anderson, Lynn Dees, James S. Tweddell, Diane E. Spicer, Andrew N. Redington*
- Video 35.11 MRI of a 6-year-old child with tetralogy of Fallot**, *Christian Apitz, Robert H. Anderson, Lynn Dees, James S. Tweddell, Diane E. Spicer, Andrew N. Redington*
- Video 35.12 MRI of a 27-year-old patient with tetralogy of Fallot**, *Christian Apitz, Robert H. Anderson, Lynn Dees, James S. Tweddell, Diane E. Spicer, Andrew N. Redington*
- Video 35.13 3D reconstruction MRI in a young adolescent with tetralogy of Fallot/pulmonary atresia/major aortopulmonary collateral arteries**, *Christian Apitz, Robert H. Anderson, Lynn Dees, James S. Tweddell, Diane E. Spicer, Andrew N. Redington*
- Video 35.14 3D CT virtual fluoroscopic image with endocast overlay of a patient with repaired tetralogy of Fallot**, *Christian Apitz, Robert H. Anderson, Lynn Dees, James S. Tweddell, Diane E. Spicer, Andrew N. Redington* (Courtesy Justin T. Tretter)
- Video 35.15 3D CT virtual dissection reconstruction of a patient with repaired tetralogy of Fallot**, *Christian Apitz, Robert H. Anderson, Lynn Dees, James S. Tweddell, Diane E. Spicer, Andrew N. Redington* (Courtesy Justin T. Tretter)
- Video 35.16 Complete repair with transannular patch**, *Christian Apitz, Robert H. Anderson, Lynn Dees, James S. Tweddell, Diane E. Spicer, Andrew N. Redington*
- Video 35.17 Right ventriculogram in a patient with repaired tetralogy of Fallot and supravulvar pulmonary stenosis**, *Christian Apitz, Robert H. Anderson, Lynn Dees, James S. Tweddell, Diane E. Spicer, Andrew N. Redington* (Courtesy Justin T. Tretter)
- Video 35.18 Right ventriculogram in a patient with repaired tetralogy of Fallot and supravulvar pulmonary stenosis**, *Christian Apitz, Robert H. Anderson, Lynn Dees, James S. Tweddell, Diane E. Spicer, Andrew N. Redington* (Courtesy Justin T. Tretter)
- Video 35.19 Balloon sizing of the supravulvar pulmonary stenosis**, *Christian Apitz, Robert H. Anderson, Lynn Dees, James S. Tweddell, Diane E. Spicer, Andrew N. Redington* (Courtesy Justin T. Tretter)
- Video 35.20 Right ventriculogram in the patient assessed in Videos 35.14, 35.15, and 35.17 through 35.19 following transcatheter pulmonary valve placement**, *Christian Apitz, Robert H. Anderson, Lynn Dees, James S. Tweddell, Diane E. Spicer, Andrew N. Redington* (Courtesy Justin T. Tretter)

- Video 35.21 Right ventriculogram in the patient assessed in Videos 35.14, 35.15, and 35.17 through 35.20 following transcatheter pulmonary valve placement**, *Christian Apitz, Robert H. Anderson, Lynn Dees, James S. Tweddell, Diane E. Spicer, Andrew N. Redington* (Courtesy Justin T. Tretter)

Chapter 36

- Video 36.1 3D MRI reconstruction of tetralogy of Fallot with pulmonary atresia and major aortopulmonary collateral arteries**, *Ritu Asija, Michael Ma, Lisa Wise-Faberowski, Laura Presnell, Robert H. Anderson, Doff B. McElhinney, Frank L. Hanley* (Courtesy Lars Grosse-Wortmann)
- Video 36.2 Descending aortic angiogram demonstrating major aortopulmonary collateral arteries**, *Ritu Asija, Michael Ma, Lisa Wise-Faberowski, Laura Presnell, Robert H. Anderson, Doff B. McElhinney, Frank L. Hanley*
- Video 36.3 Balloon occlusion angiograms of major aortopulmonary collateral arteries**, *Ritu Asija, Michael Ma, Lisa Wise-Faberowski, Laura Presnell, Robert H. Anderson, Doff B. McElhinney, Frank L. Hanley*
- Video 36.4 Balloon occlusions angiograms of major aortopulmonary collateral arteries**, *Ritu Asija, Michael Ma, Lisa Wise-Faberowski, Laura Presnell, Robert H. Anderson, Doff B. McElhinney, Frank L. Hanley*
- Video 36.5 Angiogram demonstrating connections between major aortopulmonary collateral arteries and central pulmonary arteries**, *Ritu Asija, Michael Ma, Lisa Wise-Faberowski, Laura Presnell, Robert H. Anderson, Doff B. McElhinney, Frank L. Hanley*
- Video 36.6 Angiogram demonstrating connections between major aortopulmonary collateral arteries and central pulmonary arteries**, *Ritu Asija, Michael Ma, Lisa Wise-Faberowski, Laura Presnell, Robert H. Anderson, Doff B. McElhinney, Frank L. Hanley*
- Video 36.7 Angiogram demonstrating connections between major aortopulmonary collateral arteries and central pulmonary arteries**, *Ritu Asija, Michael Ma, Lisa Wise-Faberowski, Laura Presnell, Robert H. Anderson, Doff B. McElhinney, Frank L. Hanley*
- Video 36.8 Angiogram demonstrating pulmonary artery anatomy after complete repair**, *Ritu Asija, Michael Ma, Lisa Wise-Faberowski, Laura Presnell, Robert H. Anderson, Doff B. McElhinney, Frank L. Hanley*
- Video 36.9 Angiogram demonstrating pulmonary artery anatomy after complete repair**, *Ritu Asija, Michael Ma, Lisa Wise-Faberowski, Laura Presnell, Robert H. Anderson, Doff B. McElhinney, Frank L. Hanley*

Chapter 37

- Video 37.1 Fetal echocardiogram demonstrating the aorta arising from the right ventricle and the pulmonary artery from the left ventricle**, *William B. Kyle, Charles D. Fraser, Diane E. Spicer, Robert H. Anderson, and Daniel J. Penny* (Courtesy Joshua Kailin)
- Video 37.2 Juxtaposed atrial appendage on echocardiogram**, *William B. Kyle, Charles D. Fraser, Diane E. Spicer, Robert H. Anderson, and Daniel J. Penny*
- Video 37.3 Subcostal short-axis echocardiographic clip of a patent oval foramen with left to right shunting in a patient with transposition of the great arteries**, *William B. Kyle, Charles D. Fraser, Diane E. Spicer, Robert H. Anderson, and Daniel J. Penny*

Video 37.4 3D rendering of LeCompte maneuver, *William B. Kyle, Charles D. Fraser, Diane E. Spicer, Robert H. Anderson, and Daniel J. Penny*

Video 37.5 Arterial switch operation, *William B. Kyle, Charles D. Fraser, Diane E. Spicer, Robert H. Anderson, and Daniel J. Penny*

Video 37.6 Arterial switch operation and Mee procedure, *David J. Barron, Oliver Stumper, William J. Brawn, Diane E. Spicer, and Robert H. Anderson*

Chapter 38

Video 38.1 Double-switch, Senning, ventricular septal defect patch closure, arterial switch operation, *David J. Barron, Oliver Stumper, William J. Brawn, Diane E. Spicer, and Robert H. Anderson*

Chapter 39

Video 39.1 Double-outlet right ventricle subaortic communication, echocardiography, *Christoph Haller, Glen S. Van Arsdell, Shi-Joon Yoo, Cecilia St George-Hyslop, Diane E. Spicer, Robert H. Anderson*

Video 39.2 Echocardiography of a patient with double-outlet left ventricle, *Christoph Haller, Glen S. Van Arsdell, Shi-Joon Yoo, Cecilia St George-Hyslop, Diane E. Spicer, Robert H. Anderson*

Video 39.3 3D printing of a patient with double-outlet right ventricle and subaortic interventricular communication without pulmonary outflow obstruction, *Christoph Haller, Glen S. Van Arsdell, Shi-Joon Yoo, Cecilia St George-Hyslop, Diane E. Spicer, Robert H. Anderson*

Video 39.4 3D printing of a patient with double-outlet right ventricle and subaortic interventricular communication with pulmonary outflow obstruction, *Christoph Haller, Glen S. Van Arsdell, Shi-Joon Yoo, Cecilia St George-Hyslop, Diane E. Spicer, Robert H. Anderson*

Video 39.5 3D printing of a patient with double-outlet right ventricle and subpulmonary interventricular communication, *Christoph Haller, Glen S. Van Arsdell, Shi-Joon Yoo, Cecilia St George-Hyslop, Diane E. Spicer, Robert H. Anderson*

Video 39.6 3D printing of a patient with double-outlet right ventricle and doubly committed interventricular communication, *Christoph Haller, Glen S. Van Arsdell, Shi-Joon Yoo, Cecilia St George-Hyslop, Diane E. Spicer, Robert H. Anderson*

Video 39.7 3D printing of a patient with double-outlet right ventricle and noncommitted interventricular communication, *Christoph Haller, Glen S. Van Arsdell, Shi-Joon Yoo, Cecilia St George-Hyslop, Diane E. Spicer, Robert H. Anderson*

Video 39.8 Nikaidoh operation with right ventricular-to-pulmonary artery conduit, *Christoph Haller, Glen S. Van Arsdell, Shi-Joon Yoo, Cecilia St George-Hyslop, Diane E. Spicer, Robert H. Anderson*

Video 39.9 3D printing in congenital heart surgery presentation, *Christoph Haller, Glen S. Van Arsdell, Shi-Joon Yoo, Cecilia St George-Hyslop, Diane E. Spicer, Robert H. Anderson*

Chapter 40

Video 40.1 Truncal valve overriding the interventricular septum, echocardiography, *Daniel J. Penny, Diane E. Spicer, Robert H. Anderson*

Video 40.2 Aortic-dominant common arterial trunk, echocardiography, *Daniel J. Penny, Diane E. Spicer, Robert H. Anderson*

Video 40.3 Bileaflet truncal valve, echocardiography, *Daniel J. Penny, Diane E. Spicer, Robert H. Anderson*

Video 40.4 Trileaflet truncal valve with muscular outlet ventricular septal defect, echocardiography, *Daniel J. Penny, Diane E. Spicer, Robert H. Anderson*

Video 40.5 Quadrileaflet truncal valve with perimembranous ventricular septal defect, echocardiography, *Daniel J. Penny, Diane E. Spicer, Robert H. Anderson*

Video 40.6 Muscular outlet ventricular septal defect, echocardiography, *Daniel J. Penny, Diane E. Spicer, Robert H. Anderson*

Video 40.7 Single coronary artery, echocardiography, *Daniel J. Penny, Diane E. Spicer, Robert H. Anderson*

Video 40.8 Apical sweep in common arterial trunk, echocardiography, *Daniel J. Penny, Diane E. Spicer, Robert H. Anderson*

Video 40.9 Subcostal short-axis sweep in common arterial trunk, echocardiography, *Daniel J. Penny, Diane E. Spicer, Robert H. Anderson*

Video 40.10 Mild truncal valve stenosis with severe regurgitation, echocardiography, *Daniel J. Penny, Diane E. Spicer, Robert H. Anderson*

Video 40.11 Suprasternal notch view of common arterial trunk, echocardiography, *Daniel J. Penny, Diane E. Spicer, Robert H. Anderson*

Video 40.12 Aortic dominant common arterial trunk complete repair, *Daniel J. Penny, Diane E. Spicer, Robert H. Anderson* (Courtesy James S. Tweddell)

Chapter 41

Video 41.1 Device occlusion of the arterial duct, *Lee N. Benson, Diane E. Spicer, Robert H. Anderson*

Video 41.2 Stenting the arterial duct in hypoplastic left heart syndrome, *Daniel J. Penny, Diane E. Spicer, Robert H. Anderson*

Video 41.3 Pulmonary valve dilation, *Daniel J. Penny, Diane E. Spicer, Robert H. Anderson*

Video 41.4 Stenting the arterial duct, *Daniel J. Penny, Diane E. Spicer, Robert H. Anderson*

Chapter 42

Video 42.1 Echocardiography of the pulmonic valve in an infant with pulmonary valve stenosis, *Jeffrey D. Dayton, Ralf J. Holzer, Robert H. Anderson*

Video 42.2 Echocardiography with color Doppler in an infant with pulmonary valve stenosis before balloon valvuloplasty, *Jeffrey D. Dayton, Ralf J. Holzer, Robert H. Anderson*

Video 42.3 Color compare echocardiography in an infant with pulmonary valve stenosis after balloon valvuloplasty, *Jeffrey D. Dayton, Ralf J. Holzer, Robert H. Anderson*

Video 42.4 Right ventricular angiography of a 5-month-old infant with pulmonary valve stenosis, *Jeffrey D. Dayton, Ralf J. Holzer, Robert H. Anderson*

Video 42.5 Right ventricular angiography of a 2-day-old infant with critical pulmonary valve stenosis, *Jeffrey D. Dayton, Ralf J. Holzer, Robert H. Anderson*

Video 42.6 Right ventricular angiography of a 15-year-old male with pulmonary valve stenosis, *Jeffrey D. Dayton, Ralf J. Holzer, Robert H. Anderson*

Video 42.7 Right ventricular angiography of an 11-year-old male with pulmonary valve stenosis, *Jeffrey D. Dayton, Ralf J. Holzer, Robert H. Anderson*

Chapter 43

- Video 43.1** Echocardiography apical view with color Doppler in a patient with pulmonary atresia with intact ventricular septum with significant tricuspid regurgitation, Michael A. Quail, Robert H. Anderson, Diane E. Spicer, Piers E.F. Daubeney
- Video 43.2** Echocardiographic apical sweep in a patient with pulmonary atresia with intact ventricular septum, Michael A. Quail, Robert H. Anderson, Diane E. Spicer, Piers E.F. Daubeney
- Video 43.3** Severe tricuspid valve and right ventricular hypoplasia, echocardiography apical view with color Doppler, Michael A. Quail, Robert H. Anderson, Diane E. Spicer, Piers E.F. Daubeney
- Video 43.4** Hypoplastic infundibulum, echocardiography parasternal short axis, Michael A. Quail, Robert H. Anderson, Diane E. Spicer, Piers E.F. Daubeney
- Video 43.5** Reversal of right coronary artery flow, ventriculocoronary fistula, echocardiography, Michael A. Quail, Robert H. Anderson, Diane E. Spicer, Piers E.F. Daubeney
- Video 43.6** Right ventricular angiogram in pulmonary atresia with intact ventricular septum, Michael A. Quail, Robert H. Anderson, Diane E. Spicer, Piers E.F. Daubeney
- Video 43.7** Radiofrequency wire position, Michael A. Quail, Robert H. Anderson, Diane E. Spicer, Piers E.F. Daubeney
- Video 43.8** Radiofrequency wire passed, Michael A. Quail, Robert H. Anderson, Diane E. Spicer, Piers E.F. Daubeney
- Video 43.9** Balloon valvuloplasty in pulmonary atresia with intact ventricular septum, Michael A. Quail, Robert H. Anderson, Diane E. Spicer, Piers E.F. Daubeney
- Video 43.10** Balloon valvuloplasty, Michael A. Quail, Robert H. Anderson, Diane E. Spicer, Piers E.F. Daubeney
- Video 43.11** Postprocedural right ventricular angiogram, Michael A. Quail, Robert H. Anderson, Diane E. Spicer, Piers E.F. Daubeney
- Video 43.12** Follow-up MRI at 10 years of age, Michael A. Quail, Robert H. Anderson, Diane E. Spicer, Piers E.F. Daubeney
- Video 43.13** Free pulmonary regurgitation following radiofrequency-assisted balloon valvuloplasty, Michael A. Quail, Robert H. Anderson, Diane E. Spicer, Piers E.F. Daubeney

Chapter 44

- Video 44.1** Echocardiography in the parasternal short-axis plane demonstrates a bicuspid aortic valve, Diane E. Spicer, Viktor Hraskaa, Robert H. Anderson, Salil Ginde, Joseph R. Block
- Video 44.2** Echocardiography in the parasternal long-axis plane demonstrates a thickened unicuspid aortic valve, Diane E. Spicer, Viktor Hraskaa, Robert H. Anderson, Salil Ginde, Joseph R. Block
- Video 44.3** Close-up of the aortic valve demonstrating the thickened valve with restricted leaflet motion, Diane E. Spicer, Viktor Hraskaa, Robert H. Anderson, Salil Ginde, Joseph R. Block
- Video 44.4** Close-up of the aortic valve with color Doppler demonstrates severe aortic valve stenosis with no evidence of aortic valve regurgitation, Diane E. Spicer, Viktor Hraskaa, Robert H. Anderson, Salil Ginde, Joseph R. Block
- Video 44.5** Echocardiography parasternal short-axis plane displays the unicuspid aortic valve with fusion of the commissures between the right and left coronary cusps, Diane E. Spicer, Viktor Hraskaa, Robert H. Anderson, Salil Ginde, Joseph R. Block

- Video 44.6** Open valvotomy of aortic valve, Diane E. Spicer, Viktor Hraskaa, Robert H. Anderson, Salil Ginde, Joseph R. Block
- Video 44.7** Hybrid approach, Diane E. Spicer, Viktor Hraskaa, Robert H. Anderson, Salil Ginde, Joseph R. Block
- Video 44.8** Echocardiography of a bicuspid aortic valve in parasternal long-axis plane, Diane E. Spicer, Viktor Hraskaa, Robert H. Anderson, Salil Ginde, Joseph R. Block
- Video 44.9** Echocardiography with color Doppler demonstrates mild aortic valve regurgitation, Diane E. Spicer, Viktor Hraskaa, Robert H. Anderson, Salil Ginde, Joseph R. Block
- Video 44.10** Tricuspidization of the unicuspid aortic valve, Diane E. Spicer, Viktor Hraskaa, Robert H. Anderson, Salil Ginde, Joseph R. Block
- Video 44.11** Ross operation, Diane E. Spicer, Viktor Hraskaa, Robert H. Anderson, Salil Ginde, Joseph R. Block
- Video 44.12** Echocardiography of supraaortic stenosis in parasternal long-axis plane, Diane E. Spicer, Viktor Hraskaa, Robert H. Anderson, Salil Ginde, Joseph R. Block
- Video 44.13** Echocardiography with color Doppler demonstrating turbulent flow in the proximal ascending aorta due to supraaortic stenosis, Diane E. Spicer, Viktor Hraskaa, Robert H. Anderson, Salil Ginde, Joseph R. Block
- Video 44.14** Symmetric three-patch technique, Diane E. Spicer, Viktor Hraskaa, Robert H. Anderson, Salil Ginde, Joseph R. Block
- Video 44.15** Symmetric nonpatch technique, Diane E. Spicer, Viktor Hraskaa, Robert H. Anderson, Salil Ginde, Joseph R. Block
- Video 44.16** Echocardiography in the parasternal long-axis plane, Diane E. Spicer, Viktor Hraskaa, Robert H. Anderson, Salil Ginde, Joseph R. Block
- Video 44.17** Echocardiography long-axis plane with color Doppler showing evidence of subaortic stenosis with flow turbulence, Diane E. Spicer, Viktor Hraskaa, Robert H. Anderson, Salil Ginde, Joseph R. Block
- Video 44.18** Resection of a discrete subaortic membrane with myectomy, Diane E. Spicer, Viktor Hraskaa, Robert H. Anderson, Salil Ginde, Joseph R. Block
- Video 44.19** Ross-Konno operation with resection of endocardial fibroelastosis, Diane E. Spicer, Viktor Hraskaa, Robert H. Anderson, Salil Ginde, Joseph R. Block

Chapter 45

- Video 45.1** 3D CT of repaired type B interrupted aortic arch with aberrant right subclavian, Kyle W. Riggs, Robert H. Anderson, Diane E. Spicer, David L.S. Morales
- Video 45.2** Echocardiography of discrete coarctation of the aorta, Kyle W. Riggs, Robert H. Anderson, Diane E. Spicer, David L.S. Morales
- Video 45.3** Echocardiography of coarctation with hypoplasia of the aortic arch, Kyle W. Riggs, Robert H. Anderson, Diane E. Spicer, David L.S. Morales
- Video 45.4** Echocardiography of type A interrupted aortic arch, Kyle W. Riggs, Robert H. Anderson, Diane E. Spicer, David L.S. Morales
- Video 45.5** Echocardiography of type B interrupted aortic arch, Kyle W. Riggs, Robert H. Anderson, Diane E. Spicer, David L.S. Morales

- Video 45.6** **Surgical repair of coarctation of the aorta with coarctectomy and end-to-end anastomosis**, Kyle W. Riggs, Robert H. Anderson, Diane E. Spicer, David L.S. Morales
- Video 45.7** **Aortogram demonstrating catheter crossing a severe discrete coarctation of the aorta**, Kyle W. Riggs, Robert H. Anderson, Diane E. Spicer, David L.S. Morales
- Video 45.8** **Aortogram of native coarctation of the aorta after stent deployment**, Kyle W. Riggs, Robert H. Anderson, Diane E. Spicer, David L.S. Morales
- Video 45.9** **Repair of Interrupted aortic arch (type B) and ventricular septal defect**, Kyle W. Riggs, Robert H. Anderson, Diane E. Spicer, David L.S. Morales
- Video 45.10** **Animation of Interrupted aortic arch repair**, Kyle W. Riggs, Robert H. Anderson, Diane E. Spicer, David L.S. Morales (Courtesy Drs. Moore, Morales, and Tegtmeyer)

Chapter 46

- Video 46.1** **Echocardiography in short axis showing a left main coronary artery arising from the lateral aspect of the pulmonary trunk**, Joyce Johnson, Matthew Harris, Robert H. Anderson, Diane E. Spicer, Marshall Jacobs, James S. Tweddell, Julie Brothers
- Video 46.2** **Echocardiography in short axis with color Doppler showing a left main coronary artery arising from the lateral aspect of the pulmonary trunk**, Joyce Johnson, Matthew Harris, Robert H. Anderson, Diane E. Spicer, Marshall Jacobs, James S. Tweddell, Julie Brothers
- Video 46.3** **CT showing axial images of a left coronary artery arising from the right sinus of Valsalva**, Joyce Johnson, Matthew Harris, Robert H. Anderson, Diane E. Spicer, Marshall Jacobs, James S. Tweddell, Julie Brothers
- Video 46.4** **CT showing virtual angiography of a right coronary artery arising from the left sinus of Valsalva**, Joyce Johnson, Matthew Harris, Robert H. Anderson, Diane E. Spicer, Marshall Jacobs, James S. Tweddell, Julie Brothers
- Video 46.5** **Angiogram demonstrating congenital orificial atresia of the left main coronary artery**, Joyce Johnson, Matthew Harris, Robert H. Anderson, Diane E. Spicer, Marshall Jacobs, James S. Tweddell, Julie Brothers
- Video 46.6** **Direct translocation repair of ALCAPA**, James S. Tweddell

Chapter 47

- Video 47.1** **Double aortic arch with atretic left segment; division of ductal ligament and division and ligation of atretic left aortic arch**, Roosevelt Bryant III, Shi-Joon Yoo
- Video 47.2** **Right aortic arch with aberrant left subclavian artery and diverticulum of Kommerell, division of ductal ligament**, Roosevelt Bryant III, Shi-Joon Yoo

Chapter 48

- Video 48.1** **Echocardiography of a double-barreled aorta**, Robert H. Anderson, Diane E. Spicer

Chapter 51

- Video 51.1** **Aortopulmonary window–transpulmonary patch closure**, Athar M. Qureshi, Srinath T. Gowda, Henri Justino, Diane E. Spicer, Robert H. Anderson (Courtesy David Lehenbauer)

Chapter 52

- Video 52.1** **Echocardiography of a rhabdomyoma of the left ventricular outflow tract**, Juan Carlos Muniz
- Video 52.2** **MRI first-pass perfusion of a large left ventricular vascular tumor**, Juan Carlos Muniz
- Video 52.3** **Echocardiography of a malignant secondary cardiac tumor**, Juan Carlos Muniz
- Video 52.4** **Echocardiography of a malignant secondary cardiac tumor**, Juan Carlos Muniz
- Video 52.5** **Left atrial myxoma demonstrated by transesophageal echocardiography**, Juan Carlos Muniz
- Video 52.6** **Right atrial myxoma demonstrated by transesophageal echocardiography**, Juan Carlos Muniz
- Video 52.7** **Echocardiography of a vascular tumor**, Juan Carlos Muniz
- Video 52.8** **Echocardiography of a vascular tumor**, Juan Carlos Muniz
- Video 52.9** **Coronary angiography demonstrating perfusion of vascular tumor**, Juan Carlos Muniz
- Video 52.10** **Surgical resection of myxoma**, Juan Carlos Muniz (Courtesy Juan Carlos Muniz and Kristine J. Guleserian)

Chapter 53

- Video 53.1** **MRI cine demonstrating depressed LV systolic function with regional hypokinesis**, Audrey Dionne, Annette Baker, Jane W. Newburger
- Video 53.2** **Angiogram demonstrating a giant aneurysm of the left anterior descending coronary artery**, Audrey Dionne, Annette Baker, Jane W. Newburger
- Video 53.3** **Angiogram demonstrating a giant aneurysm of the left anterior descending artery with severe stenosis at its egress**, Audrey Dionne, Annette Baker, Jane W. Newburger
- Video 53.4** **Angiogram demonstrating a giant aneurysm in the proximal right coronary artery**, Audrey Dionne, Annette Baker, Jane W. Newburger
- Video 53.5** **Angiogram demonstrating a patent coronary artery bypass graft**, Audrey Dionne, Annette Baker, Jane W. Newburger
- Video 53.6** **Coronary arterial bypass graft**, Audrey Dionne, Annette Baker, Jane W. Newburger (Courtesy James S. Tweddell)

Chapter 56

- Video 56.1** **Infective endocarditis, Case 1**, Georgi Christov, Garth Dixon, Martin Kostolny
- Video 56.2** **Infective endocarditis, Case 1**, Georgi Christov, Garth Dixon, Martin Kostolny
- Video 56.3** **Infective endocarditis, Case 1**, Georgi Christov, Garth Dixon, Martin Kostolny
- Video 56.4** **Infective endocarditis, Case 1**, Georgi Christov, Garth Dixon, Martin Kostolny
- Video 56.5** **Infective endocarditis, Case 1**, Georgi Christov, Garth Dixon, Martin Kostolny
- Video 56.6** **Infective endocarditis, Case 1**, Georgi Christov, Garth Dixon, Martin Kostolny
- Video 56.7** **Infective endocarditis, Case 1**, Georgi Christov, Garth Dixon, Martin Kostolny

- Video 56.8** **Infective endocarditis, Case 1**, Georgi Christov, Garth Dixon, Martin Kostolny
- Video 56.9** **Infective endocarditis, Case 1**, Georgi Christov, Garth Dixon, Martin Kostolny
- Video 56.10** **Infective endocarditis, Case 1**, Georgi Christov, Garth Dixon, Martin Kostolny
- Video 56.11** **Infective endocarditis, Case 2**, Georgi Christov, Garth Dixon, Martin Kostolny
- Video 56.12** **Infective endocarditis, Case 2**, Georgi Christov, Garth Dixon, Martin Kostolny
- Video 56.13** **Infective endocarditis, Case 2**, Georgi Christov, Garth Dixon, Martin Kostolny
- Video 56.14** **Infective endocarditis, Case 2**, Georgi Christov, Garth Dixon, Martin Kostolny
- Video 56.15** **Infective endocarditis, Case 3**, Georgi Christov, Garth Dixon, Martin Kostolny
- Video 56.16** **Infective endocarditis, Case 4**, Georgi Christov, Garth Dixon, Martin Kostolny
- Video 56.17** **Infective endocarditis, Case 4**, Georgi Christov, Garth Dixon, Martin Kostolny
- Video 56.18** **Infective endocarditis, Case 4**, Georgi Christov, Garth Dixon, Martin Kostolny
- Video 56.19** **Infective endocarditis, Case 4**, Georgi Christov, Garth Dixon, Martin Kostolny
- Video 56.20** **Infective endocarditis, Case 5**, Georgi Christov, Garth Dixon, Martin Kostolny
- Video 56.21** **Infective endocarditis, Case 5**, Georgi Christov, Garth Dixon, Martin Kostolny
- Video 56.22** **Infective endocarditis, Case 6**, Georgi Christov, Garth Dixon, Martin Kostolny
- Video 56.23** **Infective endocarditis, Case 6**, Georgi Christov, Garth Dixon, Martin Kostolny
- Video 56.24** **Infective endocarditis, Case 6**, Georgi Christov, Garth Dixon, Martin Kostolny
- Video 56.25** **Infective endocarditis, Case 6**, Georgi Christov, Garth Dixon, Martin Kostolny
- Video 56.26** **Infective endocarditis, Case 6**, Georgi Christov, Garth Dixon, Martin Kostolny
- Video 56.27** **Infective endocarditis, Case 7**, Georgi Christov, Garth Dixon, Martin Kostolny
- Video 56.28** **Infective endocarditis, Case 7**, Georgi Christov, Garth Dixon, Martin Kostolny
- Video 56.29** **Infective endocarditis, Case 7**, Georgi Christov, Garth Dixon, Martin Kostolny
- Video 56.30** **Infective endocarditis, Case 7**, Georgi Christov, Garth Dixon, Martin Kostolny
- Video 56.31** **Infective endocarditis, Case 7**, Georgi Christov, Garth Dixon, Martin Kostolny
- Video 56.32** **Infective endocarditis, Case 8**, Georgi Christov, Garth Dixon, Martin Kostolny
- Video 56.33** **Infective endocarditis, Case 8**, Georgi Christov, Garth Dixon, Martin Kostolny
- Video 56.34** **Infective endocarditis, Case 8**, Georgi Christov, Garth Dixon, Martin Kostolny
- Video 56.35** **Infective endocarditis, Case 8**, Georgi Christov, Garth Dixon, Martin Kostolny

Video 56.36 **Infective endocarditis, Case 8**, Georgi Christov, Garth Dixon, Martin Kostolny

Video 56.37 **Infective endocarditis, Case 9**, Georgi Christov, Garth Dixon, Martin Kostolny

Video 56.38 **Infective endocarditis, Case 9**, Georgi Christov, Garth Dixon, Martin Kostolny

Video 56.39 **Infective endocarditis, Case 9**, Georgi Christov, Garth Dixon, Martin Kostolny

Video 56.40 **Infective endocarditis, Case 10**, Georgi Christov, Garth Dixon, Martin Kostolny

Video 56.41 **Infective endocarditis, Case 10**, Georgi Christov, Garth Dixon, Martin Kostolny

Video 56.42 **Melody valve endocarditis; Melody valve and AICD lead extraction with right ventricular outflow tract reconstruction and tricuspid valve repair**, Georgi Christov, Garth Dixon, Martin Kostolny (Courtesy James S. Tweddell)

Video 56.43 **Mitral valve replacement for mitral valve endocarditis**, Georgi Christov, Garth Dixon, Martin Kostolny (Courtesy James S. Tweddell)

Chapter 57

Video 57.1 **Echocardiography in modified parasternal long-axis view showing mild pericardial effusion**, Saurabh K. Gupta

Video 57.2 **Echocardiography in apical four-chamber view during pericardiocentesis** Saurabh K. Gupta

Chapter 58

Video 58.1 **Aortic root replacement (27 mm On-X mechanical valved conduit) in Marfan syndrome**, Charles D. Fraser III, Luca A. Vricella, Duke E. Cameron (Courtesy James S. Tweddell)

Video 58.2 **Valve-sparing root reconstruction and replacement of proximal ascending aorta using a 32 mm sinus of Valsalva graft in Loeys-Dietz syndrome**, Charles D. Fraser III, Luca A. Vricella, Duke E. Cameron (Courtesy James S. Tweddell)

Chapter 62

Video 62.1 **Acute cancer treatment-related cardiotoxicity, echocardiography apical four-chamber view**, Thomas D. Ryan (Courtesy Callie Rzasa)

Video 62.2 **Acute cancer treatment-related cardiotoxicity, echocardiography parasternal short-axis view**, Thomas D. Ryan (Courtesy Callie Rzasa)

Video 62.3 **Chronic-progressive cancer treatment-related cardiotoxicity, MRI**, Thomas D. Ryan

Chapter 63

Video 63.1 **Case 1: Depressed left ventricular systolic function, echocardiography apical four-chamber view**, Deepa Mokshagundam, John Torrey Berger III

Video 63.2 **Case 1: Depressed left ventricular systolic function, echocardiography apical four-chamber view**, Deepa Mokshagundam, John Torrey Berger III

Video 63.3 **Case 1: Cannulation to ECMO. Depressed left ventricular systolic function, echocardiography apical four-chamber view**, Deepa Mokshagundam, John Torrey Berger III

- Video 63.4** **Case 1: Improved left ventricular systolic function following decannulation from ECMO, echocardiography apical four-chamber view**, Deepa Mokshagundam, John Torrey Berger III

Chapter 64

- Video 64.1** **Extracorporeal membrane oxygenation educational animation**, Saul Flores, Barbara A. Elias, Lara S. Shekerdemian
- Video 64.2** **Extracorporeal membrane oxygenation and mechanical ventilation educational animation**, Saul Flores, Barbara A. Elias, Lara S. Shekerdemian
- Video 64.3** **Pericardial effusion while on ventricular assist device, echocardiography**, Saul Flores, Barbara A. Elias, Lara S. Shekerdemian
- Video 64.4** **Ventricle function assessment after ventricular assist device explant, echocardiography**, Saul Flores, Barbara A. Elias, Lara S. Shekerdemian
- Video 64.5** **Extracorporeal membrane oxygenation circuit components**, Saul Flores, Barbara A. Elias, Lara S. Shekerdemian, MHA Texas Children's Hospital

Chapter 66

- Video 66.1** **SynCardia total artificial heart implant**, Joseph W. Rossano, Kyle W. Riggs, Kelley D. Miller, David L.S. Morales (Courtesy David L.S. Morales)
- Video 66.2** **HeartMate 3 implant**, Joseph W. Rossano, Kyle W. Riggs, Kelley D. Miller, David L.S. Morales (Courtesy David L.S. Morales)

Chapter 67

- Video 67.1** **Orthotopic, bicaval heart transplant**, Anne I. Dipchand, Julie Schmidt, Richard Kirk (Courtesy James S. Tweddell)
- Video 67.2** **Heart-lung transplant (en bloc)**, Anne I. Dipchand, Julie Schmidt, Richard Kirk (Courtesy James S. Tweddell)

Chapter 70

- Video 70.1** **Angiogram of venovenous collateral**, Joshua P. Kanter
- Video 70.2** **Angiogram of venovenous collateral**, Joshua P. Kanter
- Video 70.3** **Angiogram following occlusion of venovenous collateral**, Joshua P. Kanter
- Video 70.4** **Angiogram following occlusion of venovenous collateral**, Joshua P. Kanter
- Video 70.5** **Angiogram of collateral to the coronary sinus**, Joshua P. Kanter

Chapter 71

- Video 71.1** **Norwood with right modified BT shunt**, James S. Tweddell, Ronald A. Bronicki, Joshua W. Salvin, Maryam Y. Naim, Christine M. Riley, Gil Wernovsky (Courtesy James S. Tweddell)
- Video 71.2** **Bidirectional Glenn; right modified BT shunt takedown**, James S. Tweddell, Ronald A. Bronicki, Joshua W. Salvin, Maryam Y. Naim, Christine M. Riley, Gil Wernovsky (Courtesy James S. Tweddell)
- Video 71.3** **Extracardiac, nonfenestrated Fontan**, James S. Tweddell, Ronald A. Bronicki, Joshua W. Salvin, Maryam Y. Naim, Christine M. Riley, Gil Wernovsky (Courtesy James S. Tweddell)

Chapter 73

- Video 73.1** **MRI cine demonstrating low flow in Fontan pathway**, Thomas L. Gentles
- Video 73.2** **Fontan pathway thrombus, echocardiography**, Thomas L. Gentles
- Video 73.3** **Echocardiographic interrogation of Fontan fenestration**, Thomas L. Gentles
- Video 73.4** **Echocardiographic interrogation of Fontan fenestration following device occlusion**, Thomas L. Gentles
- Video 73.5** **Angiogram during Fontan fenestration device closure**, Thomas L. Gentles
- Video 73.6** **Angiogram after Fontan fenestration device closure**, Thomas L. Gentles
- Video 73.7** **Angiogram demonstrating a diffusely hypoplastic left pulmonary artery in a patient with bidirectional Glenn**, Thomas L. Gentles
- Video 73.8** **Angiogram demonstrating narrowing of a lateral tunnel Fontan**, Thomas L. Gentles
- Video 73.9** **Angiogram following stent placement in the diffusely hypoplastic left pulmonary artery and lateral tunnel Fontan narrowing**, Thomas L. Gentles

Chapter 75

- Video 75.1** **Depressed right ventricular systolic function, echocardiography**, Bryan Siegel, John Torrey Berger III
- Video 75.2** **Depressed right ventricular systolic function, echocardiography**, Bryan Siegel, John Torrey Berger III

Chapter 90

- Video 90.1** **Ultrasound-guided vascular access continuous tip tracking**, Andreas W. Loepke, Kelly Grogan (Courtesy Jorge A. Galvez, Matthew A. Jolley, and Elizabeth Elliot)

1

Terminology

ROBERT H. ANDERSON and DIANE E. SPICER

Introduction

It might reasonably be thought that those who diagnose and treat patients with congenitally malformed hearts would, by now, have reached consensus concerning the most appropriate way of describing the malformations with which they are confronted. It is certainly the case that nomenclature is far less contentious now than in the previous millennium. It would be a brave person, nonetheless, who stated that the field of description and categorization was now fully resolved. It is not our intention, in this chapter, to extend these polemics. Rather, we describe our own system for description, leaving the readers to decide whether this is satisfactory for their needs. By and large, there is no right or wrong way of describing hearts, simply different ways.^{1,2} Even these different ways have been mitigated to considerable extent by the cross-mapping of existing systems.³ The ongoing differences should now be resolved simply by describing the abnormal anatomy as it is observed.

The need for a standardized approach reflects the fact that the number of individual lesions that can coexist within malformed hearts is considerable. Add to this the possibilities for combinations of lesions, and the problem of providing “pigeon holes” for each entity becomes immense. Straightforward lesions, such as septal deficiencies or valvar stenoses, are typically encountered in hearts that are otherwise structurally normal. It is when the hearts containing the lesions are themselves built in grossly abnormal fashion that difficulties are produced. If these alleged complex lesions are approached in a simple and straightforward fashion, none need be difficult to understand and describe.

The simplicity is provided by recognizing that the heart has three basic building blocks, namely the atriums, ventricular mass, and arterial trunks (Fig. 1.1). The system for description and categorization based on recognition of the limited potential for variation in each of these cardiac segments was developed independently in the 1960s by two groups: one based in the United States and led by Richard Van Praagh,¹ and the other from Mexico City, headed by Maria Victoria de la Cruz.⁴ Both of these systems concentrated on the different topologic arrangements of the components within each cardiac segment. When Van Praagh and colleagues^{5,6} introduced the concept of concordance and discordance between atriums and ventricles, they were concerned primarily with the harmony or disharmony to be found between the topologic arrangements of the atrial and ventricular components. At this time, they placed less emphasis for description on the fashion in which the atrial and ventricular chambers were joined together across the atrioventricular junctions. A similar approach, concentrating on

arterial relationships, had been taken by de la Cruz et al.⁷ when they formulated their concept of arterioventricular concordance and discordance. These approaches were understandable because it was often difficult, at that time, to determine precisely how the adjacent structures were linked together.

All was changed by the advent of cross-sectional echocardiography. Since the mid-1970s, it has been possible with precision to determine how atriums are, or are not, joined to ventricles, and similarly to establish the precise morphology found at the ventriculoarterial junctions. Our preferred system evolved concomitantly with the development of echocardiography and concentrates on the variations possible across the atrioventricular and ventriculoarterial junctions. We call this system sequential segmental analysis (see Fig. 1.1). In making such analysis, we do not ignore the segments themselves. Indeed, junctional connections cannot be established without knowledge of segmental topology.

Our system, throughout its evolution,⁸⁻¹² has followed the same basic and simple rules. From the outset, we have formulated our categories on the basis of recognizable anatomic facts, avoiding any speculative embryologic assumptions. Again, from the start, we have emphasized the features of the morphology of the cardiac components, the way they are joined or not joined together, and the relations between them, as three different facets of the cardiac make-up. The clarity of the system depends upon its design. Some argue that brevity is an important feature and have constructed formidable codifications to achieve this aim.¹³ However, in the final analysis, clarity is more important than brevity. Therefore we do not shy from using words to replace symbols, even if this requires several words. Whenever possible, we strive to use words that are as meaningful in their systematic role as in their everyday usage. In our desire to achieve optimal clarity, we have made changes in our descriptions over the years, most notably in our use of the term “univentricular heart.”^{14,15} We make no apologies for these changes because their formulation, in response to valid criticisms, has eradicated initially illogical points from our system to its advantage. It is our belief that the system now advocated is entirely logical, and we hope it is simple.

Basic Concepts of Sequential Segmental Analysis

The system we advocate depends first upon the establishment of the arrangement of the atrial chambers. Thereafter, attention is concentrated on the anatomic nature of the junctions

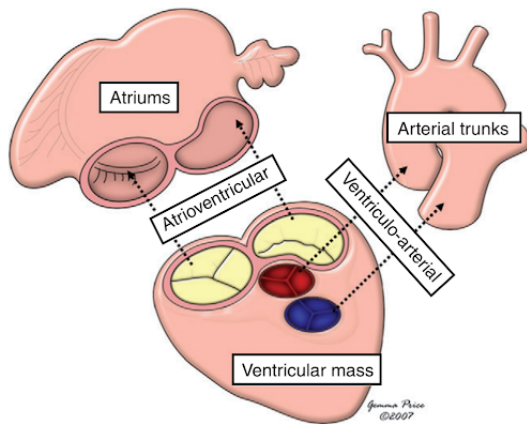


Fig. 1.1 The essence of sequential segmental analysis depends on recognition of the topologic arrangement of the three cardiac segments and combines this with analysis of the fashions in which the segments are joined, or are not joined, to each other.

between the atrial myocardium and the ventricular myocardial mass. This feature, which we describe as a type of connection, is separate from the additional feature of the morphology of the valve or valves that guard the junctions. There are two junctions in the normally constructed heart, and usually they are guarded by two separate valves. The two atrioventricular junctions can be guarded, on occasion, by a common valve. If we are to achieve this analysis of the atrioventricular junctions, we must also determine the structure, topology, and relationships of the chambers within the ventricular mass. Having dealt with the atrioventricular junctions, the ventriculoarterial junctions are also analyzed in terms of the way the arterial trunks are joined to the ventricular mass and the morphology of the arterial valves guarding their junctions. Separate attention is directed to the morphology of the outflow tracts and to the relationships of the arterial trunks. A catalog is made of all associated cardiac and, where pertinent, noncardiac, malformations. Included in this final category are such features as the location of the heart, the orientation of its apex, and the arrangement of the other thoracic and abdominal organs.

Implicit in the system is the ability to distinguish the morphology of the individual atria and ventricles and to recognize the types of arterial trunk taking origin from the ventricles. This is not as straightforward as it may seem; often, in congenitally malformed hearts, these chambers or arterial trunks may lack some of the morphologic features that most obviously characterize them in the normal heart. The most obvious feature of the morphologically left atrium in the normal heart is the connection to it of the pulmonary veins. In hearts with totally anomalous pulmonary venous connection, these veins connect in extracardiac fashion. In spite of this, it is still possible to identify the left atrium. It is considerations of this type that prompted the concept we use for recognition of the cardiac chambers and great arteries. Dubbed by Van Praagh and his colleagues the "morphologic method"¹⁶ and based on the initial work of Lev,¹⁷ the principle states that structures should be recognized in terms

of their own intrinsic morphology and that one part of the heart, which is itself variable, should not be defined on the basis of another variable structure. When this eminently sensible concept is applied to the atrial chambers, the connections of the great veins are obviously disqualified as markers of morphologic rightness or leftness because, as discussed previously, the veins do not always connect to their anticipated atria. Fortunately, there is another component of the atrial chambers that, in our experience, has been almost universally present and that, on the basis of the morphology of its junction with the remainder of the chambers, has enabled us always to distinguish between morphologically right and left atria. This is the appendage. The morphologically right appendage has the shape of a blunt triangle and joins over a broad junction with the remainder of the atrium. The junction is marked externally by the terminal groove and internally by the terminal crest. Its most significant feature is that the pectinate muscles lining the appendage extend around the parietal atrioventricular junction to reach the cardiac crux (Fig. 1.2A).

The morphologically left appendage, in contrast, is much narrower and tubular. It has a narrow junction with the remainder of the atrium, the junction being marked neither by a terminal groove nor by a muscular crest. The pectinate muscles are confined within the morphologically left appendage, with the walls of the remainder of the atrium being smooth as they extend to the cardiac crux (see Fig. 1.2B).

The morphologic method also shows its value when applied to the ventricular mass, which extends from the atrioventricular to the ventriculoarterial junctions. Within the ventricular mass as thus defined, there are almost always two ventricles. Description of ventricles, no matter how malformed they may be, is facilitated if they are analyzed as possessing three components. The first is the inlet, extending from the atrioventricular junction to the distal attachment of the atrioventricular valvar tension apparatus. The second part is the apical trabecular component. The third is the outlet component, supporting the leaflets of the arterial valve (Fig. 1.3).

Of these three components, the apical trabecular component is most universally present in normal, as well as in malformed and incomplete, ventricles. Furthermore, it is the pattern of the apical trabeculations that differentiates morphologically right from left ventricles (see Fig. 1.3). This is the case even when the apical components exist as incomplete ventricles, lacking either inlet or outlet components, or sometimes both of these components (Fig. 1.4).

When the morphology of individual ventricles is identified in this fashion, all hearts with two ventricles can be analyzed according to the way that the inlet and outlet components are shared between the apical trabecular components. To fully describe any ventricle, account must also be taken of its size. It is necessary further to describe the way that the two ventricles themselves are related within the ventricular mass. This feature is described in terms of ventricular topology because two basic patterns are found that cannot be changed without physically taking apart the ventricular components and reassembling them. The two patterns are mirror images of each other. They can be conceptualized in terms of the way that, figuratively speaking, the palmar surface of the hands can be placed upon the septal surface of the morphologically right ventricle. In the

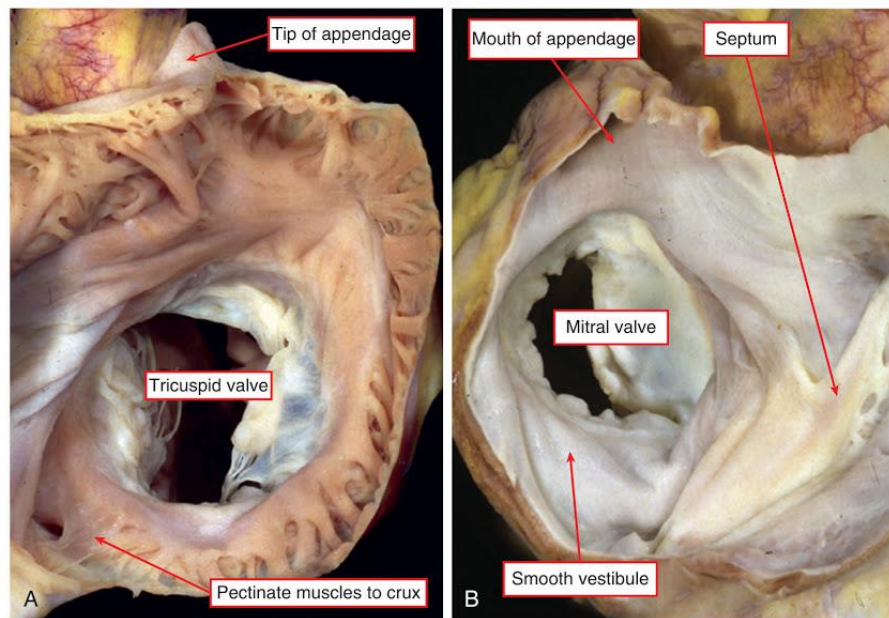


Fig. 1.2 (A) Short-axis view of the right atrioventricular junction from above, the atrium having been opened with a cut parallel to the atrioventricular junction, and with subsequent reflection of the wall of the appendage. Note that the pectinate muscles within the appendage extend all around the vestibule of the tricuspid valve. (B) Short-axis view of the left atrioventricular junction photographed from above from the same heart. The pectinate muscles are confined within the tubular appendage, so that the inferior wall of the atrium is smooth. This contains the coronary sinus within the morphologically left atrioventricular junction. Note also the typical appearance of the morphologically left side of the septum.

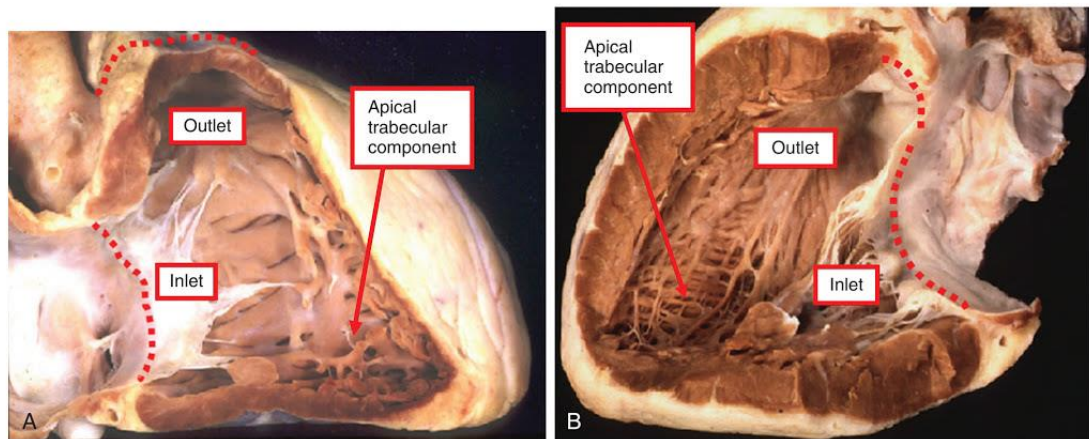


Fig. 1.3 (A) Three component parts of the morphologically right ventricle, which extends from the atrioventricular to the ventriculoarterial junctions (*dotted lines*). The coarse apical trabeculations are the most constant of these features. (B) Three component parts of the morphologically left ventricle of the same heart. The ventricular cavity again extends from the atrioventricular to the ventriculoarterial junctions (*dotted lines*). The fine apical trabeculations are its most constant feature.

morphologically right ventricle of the normal heart, irrespective of its position in space, only the palmar surface of the right hand can be placed on the septal surface such that the thumb occupies the inlet and the fingers fit into the outlet (Fig. 1.5).

Therefore the usual pattern can be described as right hand ventricular topology.¹⁸ The other pattern, the mirror

image of the right hand prototype, is described as left hand ventricular topology. In this left hand pattern, seen typically in the mirror-imaged normal heart, or in the variant of congenitally corrected transposition found with usual atrial arrangement, it is the palmar surface of the left hand that fits on the septal surface of the morphologically right ventricle with the thumb in the inlet and the fingers in

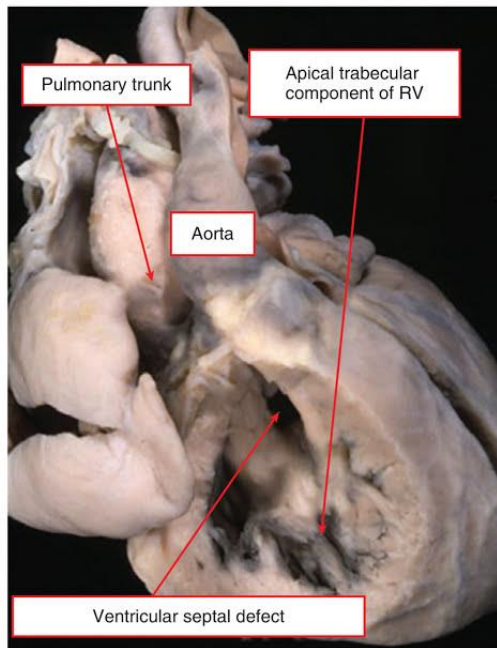


Fig. 1.4 Heart illustrating a double inlet to, and double outlet from, a dominant left ventricle. The aorta and pulmonary trunk are seen arising in parallel fashion from the left ventricle, with the aorta anterior and to the left. However, on the anterior and right-sided shoulder of the dominant left ventricle, there is still a second chamber to be seen, fed through a ventricular septal defect. This chamber is the apical trabecular component of the right ventricle (RV), identified because of its coarse trabeculations.

the outlet. This is the essence of left hand topology, or the “l-ventricular loop” (see Fig. 1.5). These two topologic patterns can always be distinguished irrespective of the location occupied in space by the ventricular mass itself. Therefore a left hand pattern of topology is readily distinguished from a ventricular mass with right hand topology in which the right ventricle has been rotated to occupy a left-sided position. Component make-up, trabecular pattern, topology, and size are independent features of the ventricles. On occasion, all may need separate description to remove any potential for confusion.

Only rarely will hearts be encountered with a solitary ventricle. Sometimes this may be because a right or left ventricle is so small that it cannot be recognized with usual clinical investigatory techniques. Nonetheless, there is a third pattern of apical ventricular morphology that is found in hearts possessing a truly single ventricle. This is when the apical component is of neither right nor left type but is very coarsely trabeculated and crossed by multiple large muscle bundles. Such a solitary ventricle has an indeterminate morphology (Fig. 1.6).

Analysis of ventricles on the basis of their apical trabeculations precludes the need to use illogically the terms “single ventricle” or “univentricular heart” for description of those hearts with one big and one small ventricle. These hearts

may produce a functionally univentricular arrangement, but all chambers that possess apical trabecular components can be described as ventricles, be they big or small and be they incomplete or complete. Any attempt to disqualify such chambers from ventricular state must lead to a system that is artificial. Only hearts with a truly solitary ventricle need be described as univentricular, albeit that the connections of the atrioventricular junctions can be univentricular in many more hearts.

When determining the morphology of the great arteries, no intrinsic features enable an aorta to be distinguished from a pulmonary trunk or from a common or solitary arterial trunk. Nonetheless, the branching pattern of the trunks themselves is sufficiently characteristic to permit these distinctions (Fig. 1.7).

The aorta gives rise to at least one coronary artery and the bulk of the systemic arteries. The pulmonary trunk gives rise directly to both, or one or other, of the pulmonary arteries. A common trunk supplies directly the coronary, systemic, and pulmonary arteries. A solitary arterial trunk exists in the absence of the proximal portion of the pulmonary trunk. In such circumstances, it is impossible to state with certainty whether the persisting trunk is common or aortic. Even in the rare cases that have transgressed one of these rules, examination of the overall branching pattern has always permitted us to distinguish the nature of the arterial trunk.

Atrial Arrangement

The cornerstone of any system of sequential analysis must be accurate establishment of atrial arrangement because this is the starting point for subsequent analysis. When arrangement of the atriums is assessed according to the morphology of the junction of the appendages with the rest of the atriums,¹⁹ there are only four possible patterns of arrangement (Fig. 1.8) because all hearts have two atrial appendages, each of which can only be morphologically left or right.

The most common is the usual arrangement, also called *situs solitus*, in which the morphologically right appendage is right-sided and the morphologically left appendage is left-sided. The second arrangement, which is very rare, is the mirror image of the usual. It is often called *situs inversus*, even though the atrial chambers are not upside down. In these two arrangements, the appendages are lateralized, with the morphologically right appendage being to one side, and the morphologically left appendage to the other. The two other arrangements do not show such lateralization. Instead, there is isomerism of the atrial appendages. In these patterns, the two appendages are mirror images of each other, with morphologic characteristics at their junctions with the rest of the atriums on both sides of either right type or left type.

Recognition of Atrial Arrangement

The arrangement of the appendages, ideally, is recognized by direct examination of the extent of the pectinate muscles

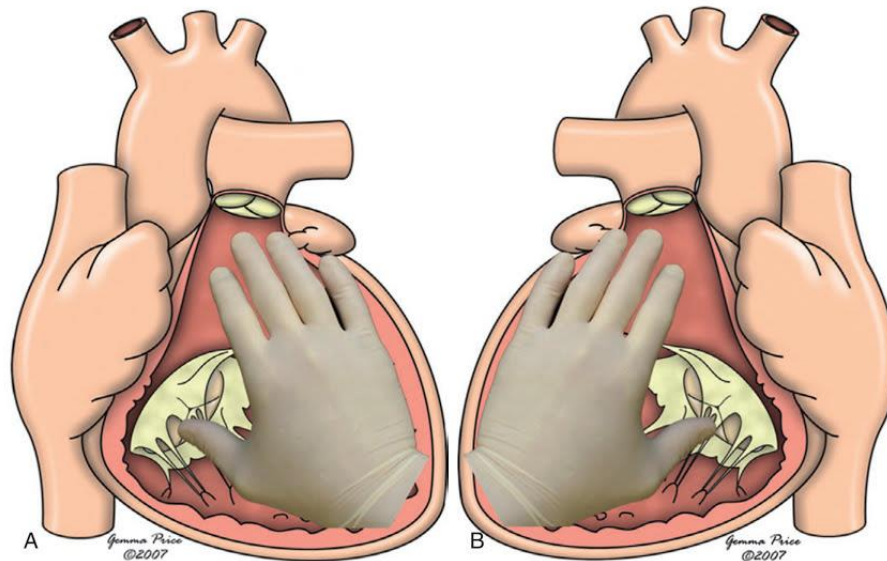


Fig. 1.5 Diagram showing how the palmar surface of the right hand can be placed on the septal surface of the normal morphologically right ventricle with the thumb in the inlet component and the fingers extending into the ventricular outlet. (A) The essence of right hand ventricular topology, also known as a d-ventricular loop. The palmar surface of the left hand fits in comparable fashion within the morphologically left ventricle, but the right hand is taken as the arbiter for the purposes of categorization. (B) The mirror-imaged normal heart. In this setting, the palmar surface of the left hand can be placed on the septal surface of the morphologically right ventricle with the thumb in the inlet and the fingers in the outlet.

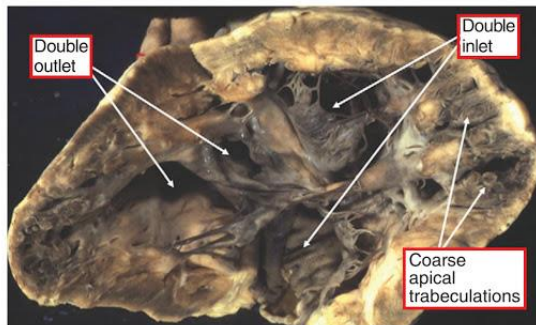


Fig. 1.6 Heart opened in clamshell fashion to show that both atrioventricular valves enter the same ventricular chamber, which also gives rise to both outflow tracts. We were unable to find a second ventricular chamber in this example. The exceedingly coarse apical trabeculations and the absence of the second chamber identify this heart as having a solitary ventricle of indeterminate morphology. This is the only true “single” ventricle.

round the vestibules (see Fig. 1.2). It has been questioned for some time as to whether these features can be distinguished in the clinical setting. With modern-day equipment, it is our belief that the arrangements should now be recognizable using cross-sectional echocardiography, particularly from the transesophageal window. The extent of the pectinate muscles can be demonstrated by using computed tomography. However, in most clinical situations, it is rarely necessary to

rely only on direct identification. This is because the morphology of the appendages is almost always in harmony with the arrangements of the thoracic and abdominal organs. In patients with lateralized arrangements, that is, the usual and mirror-imaged patterns, it is exceedingly rare for there to be disharmony between the location of the organs (Fig. 1.9).

When the appendages are isomeric, in contrast, usually the abdominal organs are typically jumbled up, although the lungs and bronchuses are typically isomeric (Fig. 1.10).

Even when there is abdominal heterotaxy, the lungs and bronchial tree are almost always symmetric. It is rare for the bronchial arrangement to show disharmony with the morphology of the appendages. The presence of isomerism therefore can almost always be inferred from the bronchial anatomy. The morphologically left bronchus is long. It branches only after it has been crossed by its accompanying pulmonary artery, making the bronchus hyparterial. In contrast, the morphologically right bronchus is short and is crossed by its pulmonary artery after it has branched, giving an eparterial pattern of branching. The four patterns of bronchial branching are almost always in harmony with the arrangement of the atrial appendages. Similar inferences to those provided from bronchial arrangement can also usually be obtained noninvasively by using cross-sectional ultrasonography to image the abdominal great vessels. These vessels bear a distinct relation to each other, and to the spine, which generally reflects bodily arrangement, although not as accurately as does bronchial anatomy. The vessels can be distinguished ultrasonically according to their pattern of

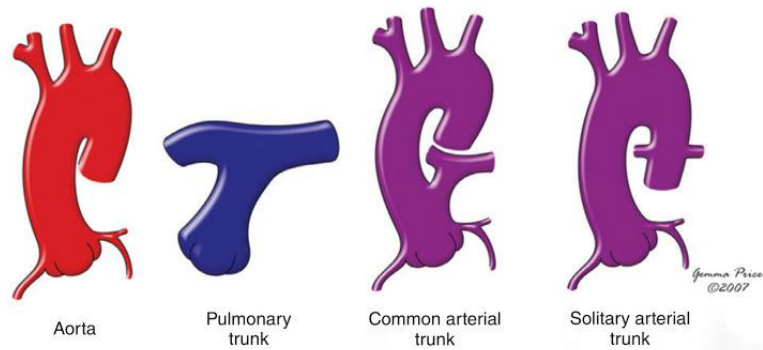


Fig. 1.7 The branching pattern of arterial trunks permits their distinction. The solitary arterial trunk is described when the intrapericardial pulmonary arteries are absent because in this setting it is impossible to determine, had they been present, whether they would have taken origin from the heart, making the trunk an aorta, or from the trunk itself, in which case there would have been a common arterial trunk with pulmonary atresia.

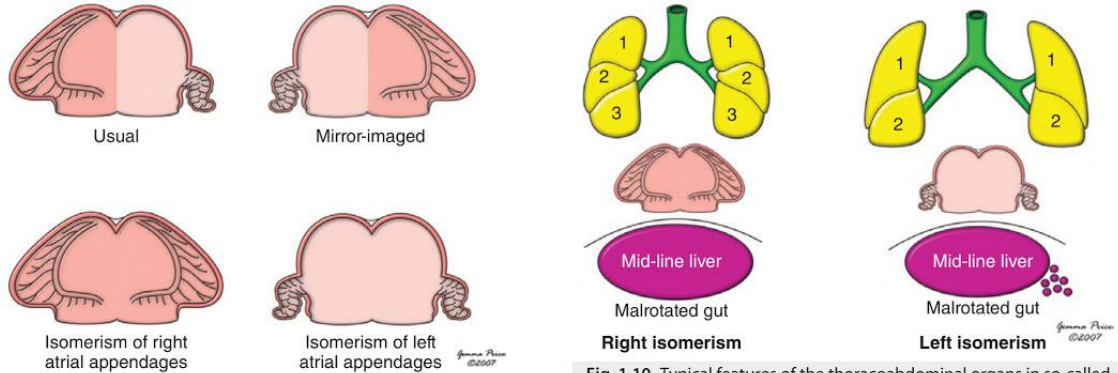


Fig. 1.8 When analyzed on the basis of the extent of the pectinate muscles relative to the atrioventricular vestibules (see Fig. 1.2), there are only four possible ways in which the two atrial appendages can be arranged. However, note that the venoatrial connections can show marked variation, particularly in the isomeric settings, also known collectively as visceral heterotaxy.

Fig. 1.10 Typical features of the thoracoabdominal organs in so-called visceral heterotaxy. The abdominal organs are jumbled up, but the lungs and atrial appendages are usually isomeric, having the same morphologic features on the right and left sides. It is usual for right isomerism to be associated with absence of the spleen and left isomerism with multiple spleens, but these associations are far from constant. Thus different pictures emerge when so-called heterotaxy is subdivided on the basis of isomerism as opposed to splenic morphology. However, cardiac assessment should start with analysis of atrial morphology based on the structure of the atrial appendages.

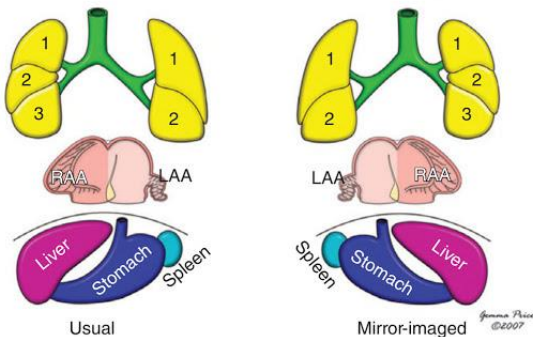


Fig. 1.9 Usual and mirror-imaged arrangements of the organs, which are lateralized. Almost always there is harmony between the arrangement of the right and left atrial appendages and the remaining thoracoabdominal organs. The numbers show the three lobes of the morphologically right and the two lobes of the morphologically left lungs. LAA, Left atrial appendage; RAA, right atrial appendage.

pulsation. When the atria are lateralized, almost without exception the inferior caval vein and aorta lie to opposite sides of the spine, with the caval vein on the side of the morphologically right appendage. When there is isomerism, the great vessels usually lie to the same side of the spine, with the caval vein in anterior position in those with isomerism of the right atrial appendages, and posterior, or with the azygos vein posterior, in those having isomerism of the left atrial appendages.

In general, isomerism of the right atrial appendages is associated with absence of the spleen, whereas isomerism of the left atrial appendages is associated with multiple spleens. Patients with isomerism of the atrial appendages therefore are frequently grouped together, from the cardiac standpoint, under the banner of the “splenic syndromes.” This approach is much less accurate than describing the

syndromes directly in terms of isomerism of the atrial appendages because the correlation between isomerism of the right atrial appendages and absence of the spleen, and between isomerism of the left atrial appendages and multiple spleens, is far from perfect.²⁰

Atrioventricular Junctions

In the normal heart, the atrial myocardium is contiguous with the ventricular mass around the orifices of the mitral and tricuspid valves. Electrical insulation is provided at these junctions by the fibrofatty atrioventricular grooves, other than at the site of the penetration of the bundle of His. To analyze accurately the morphology of the atrioventricular junctions in abnormal hearts, it is necessary to know the atrial arrangement. Equally, it is necessary to know the morphology of the ventricular mass to establish which atrium is connected to which ventricle. With this information at hand, it is possible to define the specific patterns of union or nonunion across the junctions and to determine the morphology of the valves guarding the atrioventricular junctions. In hearts with complex malformations, it is also necessary on occasion to describe the precise topology of the ventricular mass and to specify the relationships of the ventricles themselves.

Patterns of Union or Nonunion of the Atrial and Ventricular Chambers

As already described, the patterns depend on the way that the myocardium of both atria is joined to the ventricular myocardium around the entirety of the atrioventricular junctions, the atrial and ventricular muscle masses being separated from the electrical standpoint by the insulating fibrofatty tissues of the junctions other than at the site of the atrioventricular bundle. The cavities of the atrial chambers therefore are potentially connected to the underlying ventricular cavities via the atrioventricular orifices. In every heart, because there are always two atrial chambers, there is the possibility for two atrioventricular connections, which will be right sided and left sided (Fig. 1.11).

This is the case irrespective of whether the junctions themselves are guarded by two valves (see Fig. 1.11) or a common valve (Fig. 1.12).

One of the junctions may be blocked by an imperforate valvar membrane, but this does not alter the fact that, in such a setting, there are still two potential atrioventricular connections (Fig. 1.13).

In some hearts, this possibility is not fulfilled. This is because one of the connections is completely absent. In this setting the atrial myocardium on that side has no connection with the underlying ventricular myocardium, being separated from the ventricular mass by the fibrofatty tissues of the atrioventricular groove. This arrangement is the most common pattern producing atrioventricular valvar atresia (Fig. 1.14).

When atrioventricular connections are defined in this fashion, all hearts fit into one of three groups. In the first

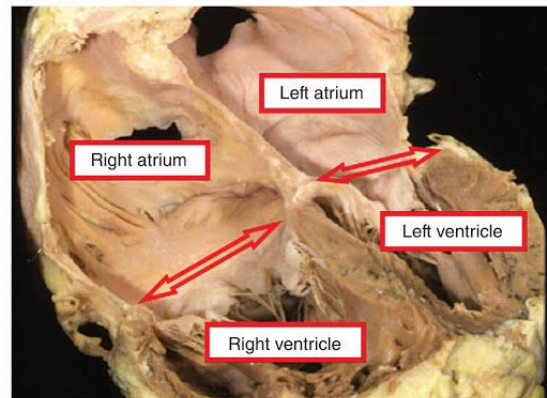


Fig. 1.11 Four-chamber section of the normal heart showing the paired atrioventricular junctions (arrows) across which the cavities of the atrial chambers are connected to their appropriate ventricles.

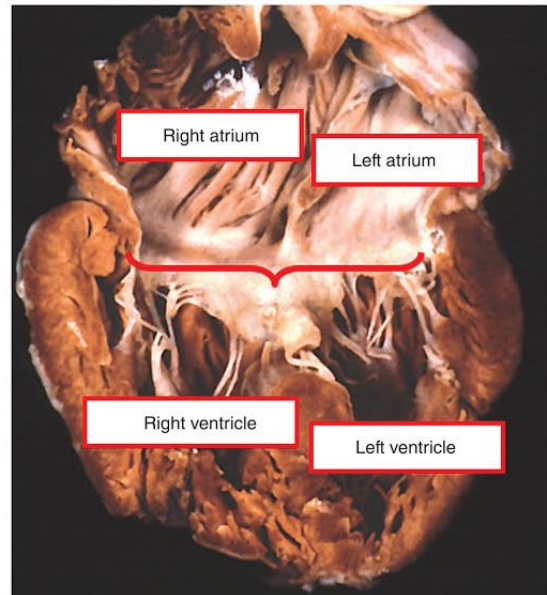


Fig. 1.12 Heart having an atrioventricular septal defect with common atrioventricular junction (bracket). However, the presence of the common junction does not disguise the fact that each atrium is joined to its own ventricle across paired junctions, albeit now guarded by a common valve.

group, by far the most common, the cavity of each atrial chamber is joined actually or potentially, but separately, to that of an underlying ventricle. The feature of the second group is that only one of the ventricles, if indeed two are present, is in communication with the atrial cavities. There is an even rarer third group. This is seen when one atrioventricular connection is absent, and the solitary atrioventricular junction, via a straddling valve, is connected to two ventricles. This arrangement is uniatrial but biventricular.

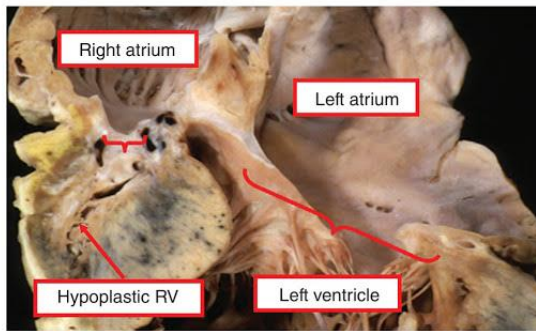


Fig. 1.13 Atrioventricular junctions sectioned in four-chamber fashion in a heart with combined tricuspid and pulmonary atresia. In this instance, unusually, the tricuspid atresia is the consequence of an imperforate right atrioventricular valve. The atrioventricular connections therefore are potentially concordant (compare with Fig. 1.14). *RV*, Right ventricle.

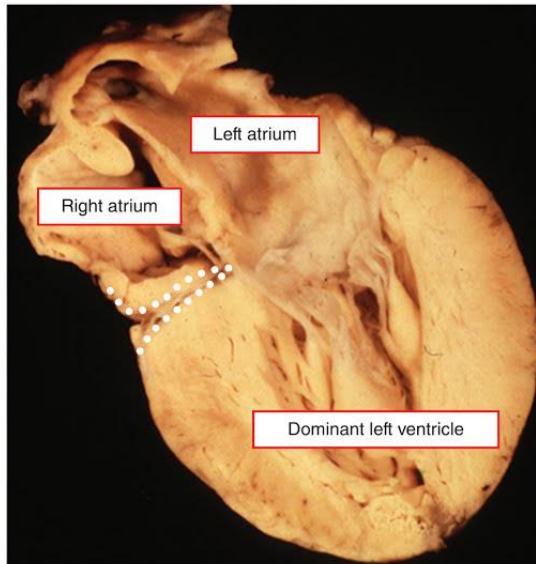


Fig. 1.14 A heart, with the usual form of tricuspid atresia, sectioned in four-chamber fashion. However, only three chambers are seen. This is because the essence of typical tricuspid atresia, and many patients with mitral atresia, is absence of an atrioventricular connection, in this instance the right atrioventricular connection (*dotted line*).

There are three possible arrangements in those hearts with each atrium joined to its own ventricle; in other words, there are three types of biventricular atrioventricular connection. These depend on the morphology of the chambers connected together. The first pattern is seen when the atria are joined to morphologically appropriate ventricles, irrespective of the topology or relationship of the ventricles or of the morphology of the valves guarding the junctions. This arrangement produces concordant atrioventricular connections. Such concordant connections can be found with either usually arranged atrial appendages or in the mirror-imaged arrangement (Fig. 1.15).

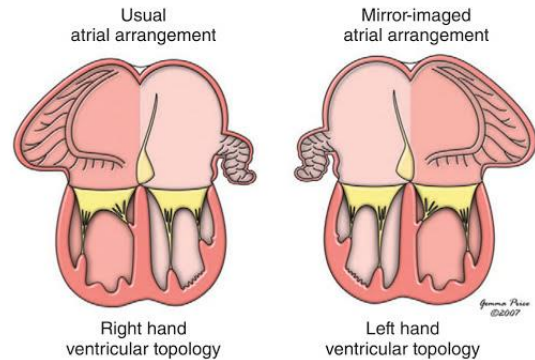


Fig. 1.15 Concordant atrioventricular connections can exist in usual and mirror-imaged patterns. Almost without exception, atria with usually arranged appendages are joined to a ventricular mass with right hand topology, whereas atria with mirror-imaged appendages are joined to a ventricular mass with left hand topology. Except when these associations are not present, it is not necessary also to state the topology of the ventricles.

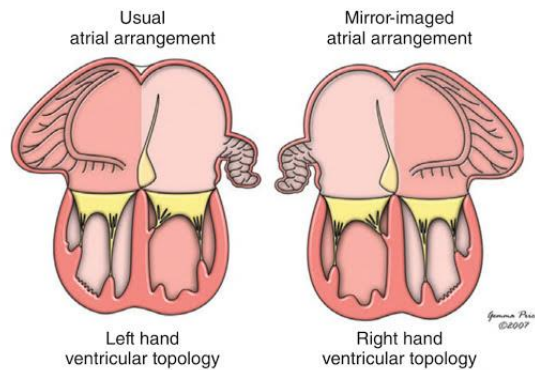


Fig. 1.16 Arrangements that, almost without exception, produce discordant atrioventricular connections.

The second arrangement, which is the reverse of the first, is again independent of relationships or valvar morphology. It produces discordant atrioventricular connections and can again be found in the usual or mirror-imaged situations. When the atrial appendages are mirror imaged in patients with discordant atrioventricular connections, the ventricles are typically in their expected pattern and, in other words, show right hand topology (Fig. 1.16).

These first two arrangements (see Figs. 1.15 and 1.16) are found when the atrial appendages are lateralized. The other biventricular atrioventricular arrangement, in which each atrium is joined to a separate ventricle, is found in hearts with isomeric appendages, whether of right or left morphology. Because of the isomeric nature of the appendages, this third arrangement cannot accurately be described in terms of concordant or discordant connections. It is a discrete biventricular pattern in its own right, which is mixed (Fig. 1.17). It, too, is independent of ventricular relationships and atrioventricular valvar morphologies and requires

specification of ventricular topology to make the description complete.

There are also three possible junctional arrangements that produce univentricular atrioventricular connections (Fig. 1.18). The first is when the cavities of right- and left-sided atrial chambers are connected directly to the same ventricle. This is called double-inlet atrioventricular connection, irrespective of whether the right- and left-sided atrioventricular junctions are guarded by two atrioventricular

valves or a common valve. The other two arrangements exist when one atrioventricular connection is absent, giving absent right-sided and absent left-sided atrioventricular connection, respectively. The patterns across the junctions that produce univentricular atrioventricular connections are different from those found with biventricular connections. Not only are they independent of ventricular relationships and valvar morphology, but they are also independent of atrial and ventricular morphologies. Hearts with concordant or discordant atrioventricular connections can exist only when usually arranged or mirror-imaged atrial chambers are each joined to separate ventricles. A heart with biventricular mixed connection can only be found when each of two atrial chambers having isomeric appendages is joined to a separate ventricle. In contrast, double-inlet, absent right-sided, or absent left-sided atrioventricular connections can be found with usually arranged, mirror-imaged, or isomeric atrial appendages. Each type of univentricular atrioventricular connection can also be found with the atriums connected to a dominant right ventricle, dominant left ventricle, or morphologically indeterminate ventricle (see Fig. 1.18).

Therefore ventricular morphology must always be described separately in those hearts in which the atrial chambers are joined to only one ventricle. In these hearts, although only one ventricle is joined to the atriums, a second ventricle is present in most of them. This second ventricle, of necessity incomplete, will be of complementary trabecular pattern to the dominant ventricle. Most frequently, the dominant ventricle is a left ventricle. The incomplete ventricle possesses right ventricular apical trabeculations. More rarely, the

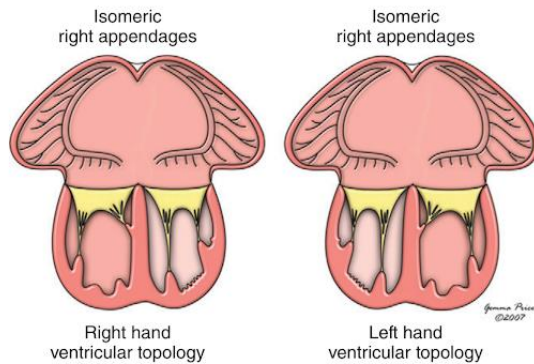


Fig. 1.17 In the setting of isomeric atrial appendages, with right isomerism as shown in the illustration, biventricular connections of necessity are mixed irrespective of ventricular topology. Therefore to fully describe these patterns, it is necessary to specify both the morphology of the atrial appendages and the ventricular topology.

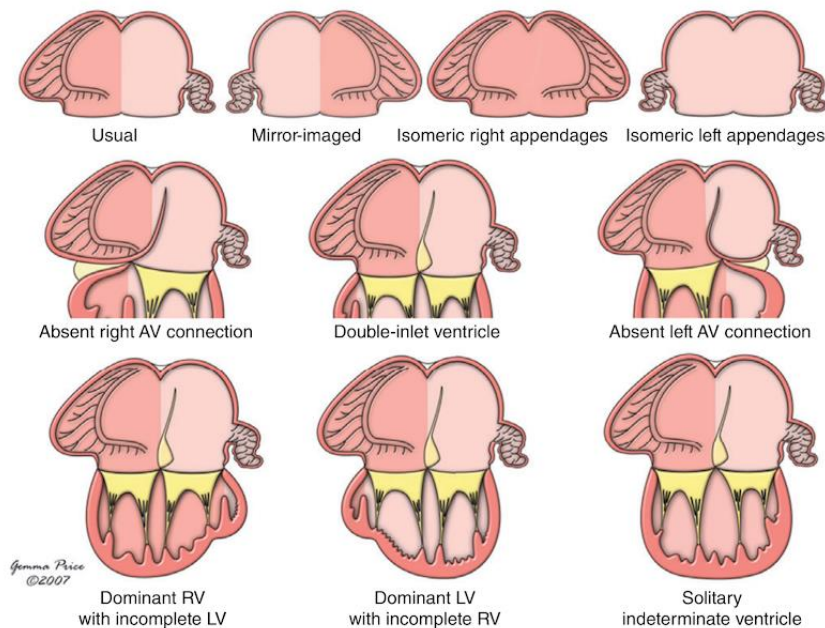


Fig. 1.18 Some of the potential univentricular atrioventricular connections. In reality, these can exist with any arrangement of the atrial appendages (top), with double-inlet, absent right, or absent left atrioventricular (AV) connections (middle), and with dominant left ventricle (LV) or right ventricle (RV), or solitary and indeterminate ventricle (bottom). The middle and bottom rows are illustrated with usual arrangement of the atrial appendages simply for convenience. There is further variability with regard to the position of the incomplete ventricle, and with ventriculoarterial connections, and so on. These hearts therefore exemplify the need for full sequential segmental analysis and description.

dominant ventricle is morphologically right, with the incomplete ventricle being morphologically left. Even more rarely, hearts will be found with a solitary ventricular chamber of indeterminate morphology (see Fig. 1.6). In clinical practice, seemingly solitary left or right ventricles may be encountered when the complementary incomplete ventricle is too small to be demonstrated.

Arrangements of the Atrioventricular Valves

Describing the fashion in which the atriums are joined to the ventricles across the atrioventricular junctions accounts only for the way in which the atrial musculature inserts into the base of the ventricular mass. The morphology of the valves guarding the overall atrioventricular junctional area is independent of this feature, within the constraints imposed by the pattern of the junctions itself. When the cavities of both atriums are joined directly to the ventricular mass, the right- and left-sided atrioventricular junctions may be guarded by two patent valves (see Fig. 1.11), by one patent valve and one imperforate valve (see Fig. 1.13), by a common valve (see Fig. 1.12), or by straddling and overriding valves (Fig. 1.19).

These arrangements of the valves can be found with concordant, discordant, biventricular and mixed, or double-inlet types of connection. Either the right- or left-sided valve may be imperforate, producing atresia but in the setting of a potential as opposed to an absent atrioventricular connection. A common valve guards both right- and left-sided atrioventricular junctions, irrespective of its morphology. A valve straddles when its tension apparatus is attached to both sides of a septum within the ventricular mass. It overrides when the atrioventricular junction is connected to ventricles on both sides of a septal structure. A right-sided valve, a left-sided valve, or a common valve can straddle, can override,

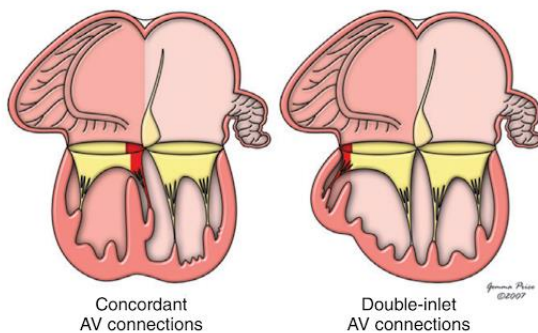


Fig. 1.19 Influence of an overriding atrioventricular (AV) junction on the precise arrangement of the connections. When the lesser part of the overriding junction is attached to the dominant ventricle, the connections are effectively biventricular and concordant in the example shown at left. In contrast, when the lesser part is committed to the incomplete ventricle, the connection is effectively double inlet and to the left ventricle in the illustration (right). Any combination of atrial chambers and ventricles can be found with such straddling and overriding valves.

or can straddle and override. Very rarely, both right- and left-sided valves may straddle and/or override in the same heart.

When one atrioventricular connection is absent, the possible modes of connection are greatly reduced. This is because there is a solitary right- or left-sided atrioventricular connection and hence a solitary atrioventricular valve. The single valve is usually committed in its entirety to one ventricle. More rarely, it may straddle, override, or straddle and override. These latter patterns produce the extremely rare group of uniaxial but biventricular connections (Fig. 1.20).

A valve that overrides has an additional influence on description. This is because the degree of commitment of the overriding atrioventricular junction to the ventricles on either side of the septum determines the precise fashion in which the atriums and ventricles are joined together. Hearts with two valves, in which one valve is overriding, are anatomically intermediate between those with, on the one hand, biventricular and, on the other hand, univentricular atrioventricular connections. There are two ways of describing such hearts. One is to consider the hearts as representing a special type of atrioventricular connection. The alternative is to recognize the intermediate nature of such hearts in a series of anomalies, and to split the series depending on the precise connection of the overriding junction. For the purposes of categorization, only the two ends of the series are labeled, with hearts in the middle being assigned to one or other of the end points. We prefer this second option (see Fig. 1.19). When most of an overriding junction is connected to a ventricle that is also joined to the other atrium, we designate the pattern as being double inlet. If the overriding junction is connected mostly to a ventricle not itself joined to the other atrium, each atrium is categorized as though joined to its own ventricle, giving the possibility of concordant, discordant, or mixed connections.

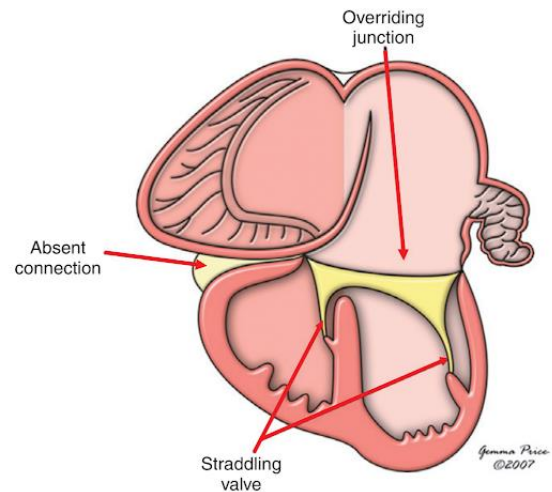


Fig. 1.20 Tricuspid atresia due to absence of the right atrioventricular connection associated with straddling and overriding of the left atrioventricular valve. This produces an atrioventricular connection that is uniaxial but biventricular. The connection can be found with any combination of atrial arrangement and ventricular topology.

When describing atrioventricular valves, it should also be noted that the adjectives “mitral” and “tricuspid” are strictly accurate only in hearts with biventricular atrioventricular connections having separate junctions, each guarded by its own valve. In this context, the tricuspid valve is always found in the morphologically right ventricle and the mitral valve in the morphologically left ventricle. In contrast, in hearts with biventricular atrioventricular connections but with a common junction, it is incorrect to consider the common valve as having mitral and tricuspid components, even when it is divided into right and left components. These right- and left-sided components, particularly on the left side, bear scant resemblance to the normal atrioventricular valves (see Chapter 36). In hearts with double inlet, the two valves are again better considered as right- and left-sided valves rather than as mitral or tricuspid. Similarly, although it is usually possible, when one connection is absent, to deduce the presumed nature of the remaining solitary valve from concepts of morphogenesis, this is not always practical or helpful. The valve can always accurately be described as being right or left sided. Potentially contentious arguments are thus defused when the right- or left-sided valve straddles in the absence of the other atrioventricular connection, giving the uniaxial but biventricular connections.

Ventricular Topology and Relationships

Even in the normal heart, the ventricular spatial relationships are complex. The inlet portions are more or less to the right and left, with the inferior part of the muscular ventricular septum lying in an approximately sagittal plane. The outlet portions are more or less anteroposteriorly related, with the septum between them in an approximately frontal plane. The apical portions extend between these two components, with the muscular septum spiraling between the inlet and outlet components. A shorthand term is needed to describe such complex spatial arrangements, and we use the concept of ventricular topology (see Fig. 1.5). In persons with usually arranged atriums and discordant atrioventricular connections, the ventricular mass almost always shows a left-handed topologic pattern, whereas right-handed ventricular topology is usually found with the combination of mirror-imaged atriums and discordant atrioventricular connections. Although these combinations are almost always present, exceptions can occur. When noting such unexpected ventricular relationships as a feature independent of the topology, we account for right-left, anterior-posterior, and superior-inferior coordinates. When necessary, we describe the position of the three ventricular components separately and relative to each other.

In hearts with disharmonious arrangements in the setting of usual atrial arrangement and discordant atrioventricular connections, the distal parts of the ventricles are usually rotated so that the morphologically right ventricular trabecular and outlet components are to the right of their morphologically left ventricular counterparts, giving the impression of “normal relationships.” In such “criss-cross” hearts seen with usual atrial arrangement and concordant atrioventricular connections, the ventricular rotation gives a spurious impression of left-handed topology. In cases with

extreme rotation, the inlet of the morphologically right ventricle may also be right sided in association with discordant atrioventricular connections. Provided relationships are described accurately and separately from the connections and the ventricular topology, none of these unusual and apparently complex hearts will be difficult either to diagnose or to categorize. In addition to these problematic criss-cross hearts, we have already discussed how description of ventricular topology is essential when accounting for the combination of isomeric appendages with biventricular mixed atrioventricular connections. This is because, in this situation, the same terms would appropriately be used to describe the heart in which the left-sided atrium was connected to a morphologically right ventricle, as well as the heart in which the left-sided atrium was connected to a morphologically left ventricle. The arrangements are differentiated simply by describing also the ventricular topology.

Both the position and the relationships of incomplete ventricles need to be described in hearts with univentricular atrioventricular connections. Here the relationships are independent of both the connections and the ventricular morphology. The incomplete right ventricle is usually anterior and right sided in classical tricuspid atresia, but it can be anterior and left sided without in any way altering the clinical presentation and hemodynamic findings. Similarly, in hearts with a double-inlet ventricle, the position of the incomplete ventricle plays only a minor role in determining the clinical presentation. Although a case can be made for interpreting such hearts with univentricular atrioventricular connections on the basis of presumed morphogenesis in the setting of right- or left-handed topologies, there are sufficient exceptions to make this approach unsuitable in the clinical setting. Therefore when we describe the position of incomplete ventricles, we simply account for their location relative to the dominant ventricle, taking note again when necessary of right-left, anterior-posterior, and superior-inferior coordinates. On occasion, it may also be advantageous to describe separately the position of apical and outlet components of an incomplete ventricle.

Ventriculoarterial Junctions

Most polemics concerning the ventriculoarterial junctions devolved upon the failure to distinguish between the way the arterial trunks arose from the ventricular mass as opposed to their relations to each other, along with undue emphasis on the nature of the infundibulum supporting their arterial valves. When these features are described independently, following the precepts of the morphologic method, all potential for disagreement is removed.

ORIGIN OF THE ARTERIAL TRUNKS FROM THE VENTRICULAR MASS

As with analysis of the atrioventricular junctions, it is necessary to account separately for the way the arteries take origin and the nature of the valves guarding the ventriculoarterial junctions. There are four possible types of origin. Concordant ventriculoarterial connections exist when the aorta arises from a morphologically left ventricle, and the pulmonary trunk from a morphologically right ventricle, be the ventricles

complete or incomplete. The arrangement where the aorta arises from a morphologically right ventricle or its rudiment, and the pulmonary trunk from a morphologically left ventricle or its rudiment, produces discordant ventriculoarterial connections. Double-outlet connection is found when both arteries are connected to the same ventricle, which may be of right ventricular, left ventricular, or indeterminate ventricular pattern. As with atrioventricular valves, overriding arterial valves (see later) are assigned to the ventricle supporting the greater parts of their circumference. The fourth ventriculoarterial connection is single outlet from the heart. This may take one of four forms. A common trunk exists when both ventricles are connected via a common arterial valve to one trunk that gives rise directly to the coronary arteries, at least one pulmonary artery, and the majority of the systemic circulation. A solitary arterial trunk exists when it is not possible to identify any remnant of an atretic pulmonary trunk within the pericardial cavity. The other forms of single outlet are single pulmonary trunk with aortic atresia or single aortic trunk with pulmonary atresia. These latter two categories describe only those arrangements in which, using clinical techniques, it is not possible to establish the precise connection of the atretic arterial trunk to a ventricular cavity. If its ventricular origin can be established but is found to be imperforate, then the connection is described, along with the presence of an imperforate valve (see later). It is also necessary in hearts with single outlet to describe the ventricular origin of the arterial trunk. This may be exclusively from a right or a left ventricle, but more usually the trunk overrides the septum, taking its origin from both ventricles.

There are fewer morphologies for the valves at the ventriculoarterial than at the atrioventricular junctions. A common arterial valve can exist only with a specific type of single outlet, namely common arterial trunk. Straddling of an arterial valve is impossible because it has no tension apparatus. Thus the possible patterns are two perforate valves, one or both of which may override, or one perforate and one imperforate valve. As with overriding atrioventricular valves, the degree of override of an arterial valve determines the precise origin of the arterial trunk from the ventricular mass, the overriding valve, or valves, being assigned to the ventricle supporting the greater part of its circumference. For example, if more than half of an overriding pulmonary valve was connected to a right ventricle, the aorta being connected to a left ventricle, we would code concordant connections. If more than half the overriding aortic valve was connected to the right ventricle in this situation, we would code double-outlet connections. In this way, we avoid the necessity for intermediate categories. Nonetheless, the precise degree of override is best stated whenever an overriding valve is found. This is done to the best of one's ability, using whichever techniques are available, and recognizing the subjective nature of the task. In this setting, as with atrioventricular connections, we err on the side of the more usually encountered pattern.

ARTERIAL RELATIONSHIPS

Relationships are usually described at valvar level, and many systems for nomenclature have been constructed on

this basis. It remains a fact that "d-transposition" is used as though synonymous with all combinations of concordant atrioventricular and discordant ventriculoarterial connections, although this was not how the term was initially used. In the same way, "l-transposition" was used as a synonym for congenitally corrected transposition. In reality, we now know that the relationships of the arterial valves are a poor guide to ventricular topology. Describing arterial valvar position in terms of leftness and rightness also takes no cognizance of anteroposterior relationships, an omission particularly because, for many years, an anterior position of the aorta was used as the cornerstone for definitions of "transposition." We prefer to describe arterial valvar relationships in terms of both right-left and anterior-posterior coordinates. Such description can be accomplished with as great a degree of precision as is required. A good system is the one that describes aortic position in degrees of the arc of a circle constructed around the pulmonary valve.¹⁸ Aortic valvar position is described relative to the pulmonary trunk in terms of eight positions of a compass, using the simple terms left, right, anterior, posterior, and side by side, in their various combinations. As long as we remember that these describe only arterial valvar relationships and convey no information about either the origin of the arterial trunks from the ventricular mass, or the morphology of the ventricular outflow tracts, we have no fear of producing confusion.

From the stance of positions of the arterial trunks, the possibilities are either for the pulmonary trunk to spiral round the aorta as it ascends from the base of the ventricles or for the two trunks to ascend in parallel fashion. Only rarely is it necessary specifically to describe these relationships. Spiraling trunks are associated most frequently with concordant ventriculoarterial connections, and parallel trunks with discordant or double-outlet connections, but again there is no predictive value in these relationships. In almost all hearts, the aortic arch crosses superiorly to the bifurcation of the pulmonary arteries.

An unexpected position of the aortic arch is a well-recognized associated anomaly of conditions such as tetralogy of Fallot (see Chapter 36) or common arterial trunk (see Chapter 41). In this respect, distinction should be made between the position of the arch and the side of the descending aorta, particularly when describing vascular rings (see Chapter 48). The side of the aortic arch depends on whether it passes to the right or left of the trachea. The position of the descending aorta is defined relative to the vertebral column.

INFUNDIBULAR MORPHOLOGY

The infundibular regions are no more and no less than the outlet components of the ventricular mass, but they have proven contentious in the realms of nomenclature. For example, in the past, the presence of bilateral conuses was considered an arbiter of the ventriculoarterial connection when associated with double-outlet right ventricle but ignored when each great artery with its complete muscular infundibulum was supported by its own ventricle. If the infundibular structures are recognized for what they are, and their morphology described as such, they provide no